Author/s

Dr. Alberto Cruz Alcalde
*Departament of Chemical
Engineering and Analytical
Chemistry, Universitat de
Barcelona*
Dr. Alessandro Amadei
*Departament Engineering, La
Sapienza, Rome, Italy*

UNIVERSITAT DE
BARCELONA

Grau en
Enginyeria
Química

Treball Final de Grau

Hydrothermal liquefaction of sewage sludge for biofuel applications: A kinetic process model and a simulation analysis.

Esteban Mujica Ruiz

(January 2025)

What we know is a drop,
what we don't know is an ocean
Isaac Newton

This research project marks the conclusion of a journey full of challenges and learning. Living in Rome and being part of La Sapienza University, one of the most prestigious institutions in Europe, has been a unique experience that allowed me to grow both academically and personally. During this time, I had the opportunity to immerse myself in a new culture, meet inspiring people, and broaden my horizons.

I would like to express my sincere gratitude to Dr. Alessandro Amadei for his guidance and expertise in the hydrothermal liquefaction of wastewater sludge. His support and patience were key to overcoming the initial challenges and advancing in this project. I also thank Dr. Benedetta DeCaprariis for her guidance and commitment, which helped me stay on track and achieve the project's goals.

A special thanks to Dr. Valentina Segneri, whose assistance with Aspen Plus simulations and kinetic modeling. Lastly, I want to thank Dr. Alberto Cruz, my supervisor at the University of Barcelona, for his constant support and motivation, even from afar.

To all of you, thank you for being a fundamental part of my learning experience and for making this journey unforgettable.

CONTENTS

SUMMARY

The present work analyzes hydrothermal liquefaction (HTL) as a sustainable and efficient method for converting sewage sludge into biocrude and other valuable products. HTL operates at moderate temperatures and pressures, allowing the direct processing of wet biomass without the need for prior drying, making it a more energy-efficient alternative to conventional waste management methods.

The study includes the identification and analysis of the reaction pathways involved in the HTL process from sewage sludge, with the objective of optimizing biocrude production. A kinetic model was developed to predict the yield of biocrude, gases, and aqueous and solid phase products under different operating conditions. The model was validated with experimental data, demonstrating high accuracy and reinforcing the viability of HTL as a scalable process.

A simulation of the HTL process was carried out using Aspen Plus v12, revealing that the optimal temperature to maximize biocrude yield is approximately 300 ºC, with a residence time of 25 minutes. Under these conditions, the process achieves a biocrude yield of around between 45% and 50%, which aligns reasonably well with experimental results showing a yield of around 30% yield.

The research highlights the potential of HTL to reduce solid waste, recover renewable energy, and support the principles of the circular economy. By addressing discrepancies between experimental and simulated results, the project provides valuable insights for the industrial-scale implementation of HTL, promoting sustainable sewage sludge management and biofuel production.

Keywords: Hydrothermal liquefaction, sewage sludge, biocrude, kinetic model, sustainable waste management, circular economy, biofuel.

RESUMEN

El presente trabajo analiza la licuefacción hidrotermal (HTL) como un método sostenible y eficiente para convertir lodos de aguas residuales en biocrudo y otros productos de valor añadido. El proceso de HTL opera a temperaturas y presiones moderadas, lo que permite el procesamiento directo de biomasa húmeda sin necesidad de un secado previo, convirtiéndolo en una alternativa más eficiente energéticamente en comparación con los métodos convencionales de gestión de residuos.

El estudio incluye la identificación y el análisis de las rutas de reacción involucradas en el proceso HTL a partir de lodos de aguas residuales, con el objetivo de optimizar la producción de biocrudo. Se desarrolló un modelo cinético para predecir el rendimiento de biocrudo, gases y productos de las fases acuosa y sólida bajo diferentes condiciones operativas. El modelo fue validado con datos experimentales, demostrando una alta precisión y reforzando la viabilidad del HTL como un proceso escalable.

Se realizó una simulación del proceso HTL utilizando Aspen Plus v12, revelando que la temperatura óptima para maximizar el rendimiento del biocrudo es aproximadamente 300 ºC, con un tiempo de residencia de 25 minutos. Bajo estas condiciones, el proceso alcanza un rendimiento de biocrudo de entre el 45% y el 50%, lo cual se alinea razonablemente bien con los resultados experimentales que muestran un rendimiento de alrededor del 30%.

La investigación destaca el potencial del HTL para reducir residuos sólidos, recuperar energía renovable y apoyar los principios de la economía circular. Al abordar las discrepancias entre los resultados experimentales y simulados, el proyecto proporciona información valiosa para la implementación a escala industrial del HTL, promoviendo una gestión sostenible de los lodos de aguas residuales y la producción de biocombustibles.

Paraules clau: Licuefacción hidrotermal, lodos residuales, biocrudo, modelo cinético, gestión sostenible de residuos, economía circular, biocombustible.

SUSTAINABLE DEVELOPMENT GOALS

This work reviews, in first place the current state of hydrothermal liquefaction (HTL) applied to sewage sludge, analyzing recent advancements and the associated technical challenges.

The project then addresses the need to find more efficient and sustainable methods for managing the excess sludge generated in wastewater treatment. Managing this waste is a significant challenge, as traditional methods such as landfilling, composting, and incineration have various limitations and contribute to environmental pollution. Moreover, these approaches overlook the potential of sludge as a renewable energy source.

The aim of this study was finally to develop a rigorous process simulation model for the hydrothermal liquefaction (HTL) of sewage sludge, enabling accurate predictions of product yields and element recovery. The model is based on global kinetics derived from laboratory-scale experiments and is implemented in Aspen Plus for the conceptual design of an HTL system integrated into a wastewater treatment plant. Initially, the model is validated with experimental data and its accuracy is later confirmed with simulations.

The project aligns with several Sustainable Development Goals (SDGs):

SDG 7: Ensure access to affordable, reliable, sustainable, and modern energy for all.

Target 7.2: Increase the share of renewable energy in the global energy mix. Promote the use of clean and renewable technologies to reduce dependence on fossil fuels and decrease greenhouse gas emissions.

Target 7.4: Facilitate investment in sustainable energy technologies and foster innovation in the energy sector.

SDG 9: Build resilient infrastructure, promote inclusive and sustainable industrialization, and foster innovation.

Target 9.2: Promote sustainable industrial practices that reduce environmental impact and encourage efficient resource use.

1. INTRODUCTION

Sewage sludge (SS) is a byproduct produced in large quantities during wastewater treatment. In China, such as, around 20 million tons are generated annually, whereas in Europe about 10 million tons are produced. Managing this waste is a major challenge, as traditional methods such as landfilling, composting, or incineration have many limitations and contribute to environmental pollution. Moreover, these approaches fail to take advantage of the sludge's potential as a source of energy or carbon. Therefore, the search for more sustainable alternatives has become increasingly important.

One interesting option is hydrothermal liquefaction (HTL), a technology that enables the valorization of sludge without requiring prior drying. Unlike methods such as pyrolysis or incineration, HTL operates at moderate temperatures and pressures, breaking down organic matter into biocrude, solid residues, water, and gas. This technology is particularly well-suited for materials with high moisture content, such as sewage sludge, as it facilitates energy recovery without relying on agricultural land that could be used for food production.

However, scaling HTL up to an industrial level remains a significant challenge. The variability in sludge composition and the complexity of the chemical reactions make it difficult to develop accurate models to optimize the process. To date, most models have primarily been based on laboratory data, limiting their ability to predict process behavior under real-world conditions. This highlights the need to develop more robust and detailed models to improve predictions.

This work reviews the current state of HTL applied to sewage sludge, analyzing the latest advancements and technical challenges. A simulation model is proposed to optimize the process using experimental data. The objective is to facilitate the industrial scaling of the technology,

enabling the production of renewable fuels, carbon recovery, and the elimination of microcontaminants and nutrients such as phosphorus.

1.1.   GENERAL ASPECTS:

The constant growth of the global population is driving an increasing demand for natural resources such as water, fossil fuels, and food. This, in turn, leads to the generation of large amounts of waste that need proper management to reduce their environmental impact. Among these wastes is sewage sludge, a semi-solid byproduct from the treatment of municipal and industrial wastewater, which can make up as much as 3% of the total volume of treated wastewater. It is estimated that the European Union produces between 10 and 13 million tons of sewage sludge (dry matter) annually, while global production reaches approximately 45 million tons [1]. This sludge is a heterogeneous mixture that contains valuable organic nutrients for agriculture, such as carbon, nitrogen, and phosphorus. However, due to the presence of heavy metals, synthetic organic compounds, and pathogens, its management requires careful precautions to minimize environmental risks.

In Europe, the main methods for managing sewage sludge include recycling for agricultural use (around 40%), incineration (about 27%), composting (approximately 10%), and landfilling (estimated at 11%, although this last option is being phased out due to stricter regulations) [2]. Additionally, there are less common methods, such as its use in forestry and land reclamation, reflecting the differences in management strategies across European countries [2]. Figure 1 clearly illustrates this variability, showing the proportion of different sludge management methods in each country. Netherlands relies almost entirely on incineration (96%) due to the ban on recycling sludge for agricultural purposes. In contrast, around 90% of sludge in Ireland and Spain is used in agriculture, reflecting a preference for its application as fertilizer. Meanwhile, in Hungary, composting is the dominant method, accounting for 74% of sludge management, while countries like Greece, Serbia, Malta, and Bosnia still depend primarily on landfilling, suggesting a lack of alternative technologies or less developed regulations.

Traditional methods of sludge management have several environmental drawbacks. Using sludge in agriculture can transfer contaminants to the soil, while incineration and landfilling release pollutants into the air, soil, and water. Although incineration allows for some energy recovery, it requires significant energy input for sludge drying, which reduces its overall efficiency
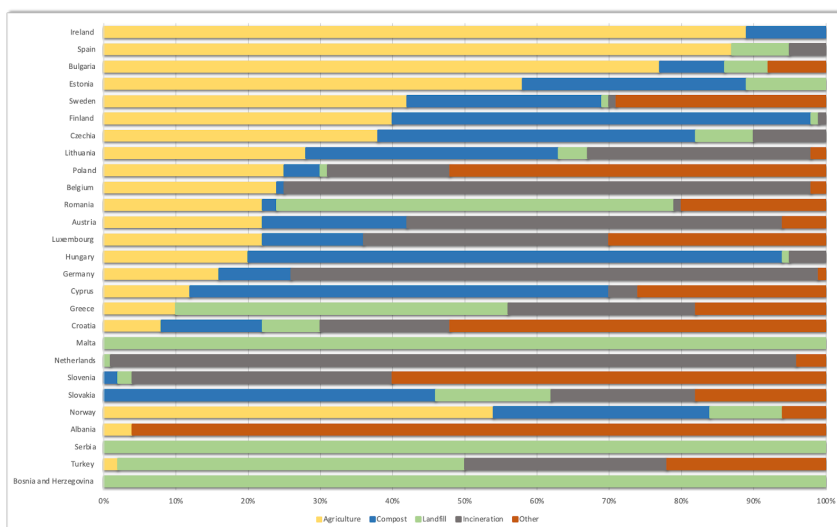
Figure 1. Removal of sewage sludge from urban WWTPs by treatment method, reporting year between 2017-2020 [1].

1.1.1.   Production

Sewage sludge is a semi-solid waste material or slurry, and it is generally classified as primary or secondary sludge. The production of sewage sludge (SS) in a wastewater treatment plant (WWTP) is shown in Figure 2. Primary sludge is obtained from chemical precipitation and sedimentation, while secondary sludge is a residue from the biological treatment process. The main objectives of treating sludge before disposal are to reduce its volume, which lower storage costs, and to stabilize its organic content to minimize chemical, biological, and toxicological risks. In most cases, dewatered sludge still contains over 80% water. Sewage sludge contains inorganic

compounds, a significant amount of nutrients, organic chemicals, as well as pathogens. Proper treatment of this sludge is considered extremely important to minimize potential environmental and social impacts [3].
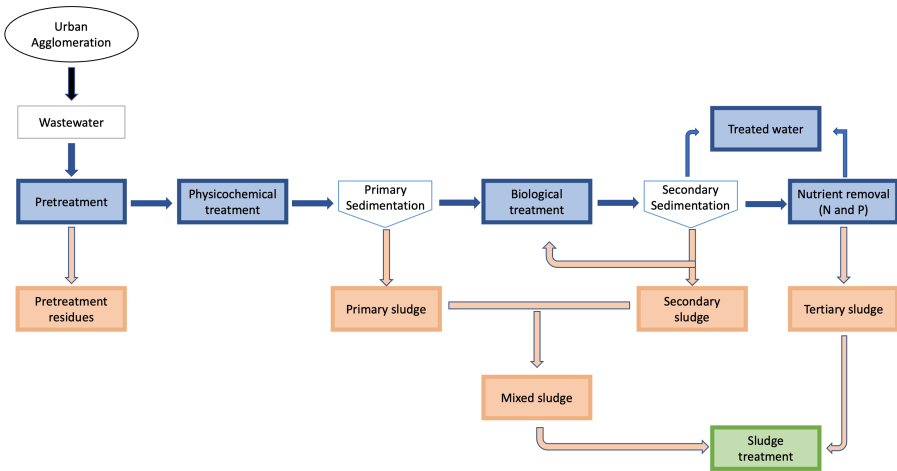
Figure 2. Flowchart of wastewater treatment and sludge production.

1.2.   SEWAGE SLUDGE TREATMENT:

There are multiple ways to treat sewage sludge (SS), with most approaches focusing on converting it into valuable resources and energy. Transforming waste into useful resources is not only efficient but also supports the principles of the circular economy, encouraging more sustainable management practices.

Traditionally, sludge disposal has involved landfilling or composting. The latter is based on the presence of nutrients like nitrogen (N), phosphorus (P), and potassium (K), which give the sludge added value as a fertilizer [4]. However, using sludge compost in agriculture carries the

risk of introducing contaminants, such as heavy metals, microplastics, and toxic chemicals, which can accumulate in the soil and eventually enter the food chain. Additionally, sludge dehydration is a critical step in the composting process, as achieving high-quality compost requires a moisture content of less than 60% [5].

Sewage sludge is also a promising source for phosphorus recovery, an essential resource for agricultural production. According to data from the European Commission, approximately 41% of the phosphorus in municipal sludge is currently recovered and reused in agriculture [6].

Moreover, the carbon content in sludge presents a unique opportunity as a raw material for producing activated carbon. Activated carbon is used in drinking water treatment plants as an efficient and cost-effective adsorbent for removing impurities and contaminants, such as organic matter, gases, and small particles [7]. However, a significant challenge is the high inorganic content of sludge, which limits the development of large surface areas in the resulting material, thereby affecting its adsorption capacity.

Figure 3 provides an overview of the different treatment methods applied to sewage sludge.
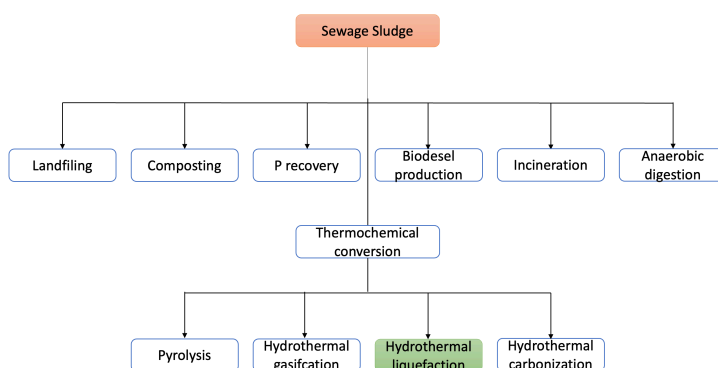
Figure 3. Multiple pathways for sewage sludge treatment.

Incineration is the most common method for disposing of sewage sludge in Netherlands, the United States, and Japan [8]. This technique significantly reduces the volume of sludge, making its disposal easier. However, one of the main challenges of incineration is the high-water content present in these sludges, which complicates their combustion. Therefore, a drying process is often needed beforehand to enhance the burning efficiency. For the sludge to be incinerated effectively without requiring additional heat, it must reach a solid content of at least 28% [9].

In contrast, anaerobic digestion offers an alternative to incineration, as it eliminates the need to dry the sludge before treatment. This biological process is widely used due to its ability to convert organic matter into biogas, a renewable energy source. However, anaerobic digestion has its drawbacks: the process is relatively slow, with fermentation times ranging from 7 days to 5 weeks. Additionally, the conversion efficiency of organic matter is usually low, limiting the overall energy yield of the process [10].

1.3.   THERMOCHEMICAL CONVERSION:

1.3.1.   Pyrolysis

Pyrolysis is a thermochemical process that breaks down organic materials through the application of heat in an environment with little or no oxygen. When the waste is subjected to temperatures typically ranging from 300°C to 900°C, these materials are transformed into various products: gases, liquids, and solids [11].

This process takes place in a closed, controlled reactor where oxygen levels are kept very low to prevent combustion. Pyrolysis consists of three main stages. The first is preheating, where the waste is heated until it reaches the temperature required to initiate decomposition. As the temperature rises, organic compounds start to release in the form of volatile products. The next stage is decomposition, during which these volatile products are separated into different fractions,

including gases, liquids, and solids [12]. Finally, in the cooling stage, the obtained products are cooled down to facilitate further processing and recovery. Techniques such as separation, extraction, or filtration are applied to refine the final products.

Pyrolysis offers significant advantages, such as a reduction in the volume of waste and the ability to generate energy from the by-products. However, one of the drawbacks of this process is its high cost. Additionally, up to 36% of the total weight of the processed waste may turn into ash, affecting the profitability of the method. Another aspect to consider is that the produced bio-oil usually has high viscosity and a high oxygen content, requiring additional improvements to optimize its quality and make it more efficient as a fuel [12].
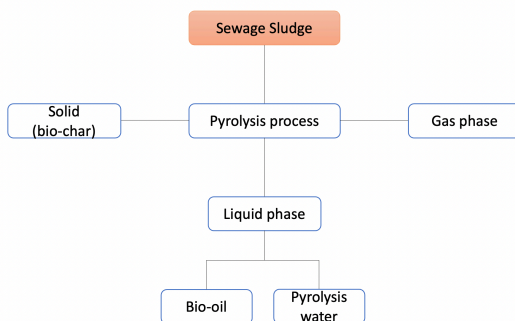
Figure 4. Result of the pyrolysis process: Syngas, bio-oil and bio-char.

1.3.2. Hydrothermal gasification

Hydrothermal gasification (HTG) is an advanced thermochemical conversion process that transforms wastewater sludge into combustible gases, taking advantage of its high-water content. Unlike pyrolysis, HTG occurs in an aqueous environment, eliminating the need for prior drying and optimizing energy use. In this process, the carbonaceous content of the material is converted into combustible gases, mainly hydrogen (H_2), through chemical reactions that take place at temperatures ranging from 400 to 1400°C and pressures of up to 40 MPa [13].

The process is carried out in a closed reactor under conditions of certain temperature and pressure, where water in its subcritical or supercritical state acts as both a solvent and a reactant. These conditions facilitate the breakdown of organic matter into gases such as hydrogen (H_2), methane (CH_4), and carbon dioxide (CO_2). Within the reactor, several key reactions occur, including hydrolysis, aqueous reforming, and methanogenesis, which convert the compounds into valuable gases [14].

However, one of the main challenges of hydrothermal gasification is the choice of reactor material. The high temperatures and the need for heat recovery require the reactor material to be highly resistant to resist extreme conditions. Additionally, high ash content in sludge interferes with complete gasification and reduce the overall efficiency of the process.

Once the reactions are complete, the produced gas is cooled and passed through a separation system where solids and impurities are removed. The gas is then purified to obtain a final product rich in hydrogen and methane, ready for use as fuel [14].

1.3.3.   Hydrothermal Carbonization

Hydrothermal carbonization (HTC) is a thermochemical process that transforms wet biomass into a carbon-rich solid product known as hydrochar. This process is carried out in a closed aqueous medium, subjecting the biomass to moderate temperatures, typically between 180ºC and 250 °C, and pressures of around 2 to 10 MPa. One of the main advantages of HTC is its ability to process materials with high moisture content without the need for prior drying, making it more energy-efficient compared to pyrolysis [15].

During HTC, the biomass undergoes various chemical and physical transformations under the applied temperature and pressure conditions. First, hydrolysis breaks the bonds in the macromolecular components of the biomass. After that, decarboxylation and dehydration reactions occur, removing functional groups in the form of carbon dioxide (CO_2) and water (H_2O), thereby increasing the relative carbon content of the resulting solid product [15]. Subsequently,

the intermediates formed in these initial stages recombine through condensation and polymerization reactions, producing carbonized structures with properties equivalent to those of natural coal.

Hydrochar, the main product of HTC, is a carbon-rich solid material with multiple applications, such as solid biofuel, adsorbent in environmental processes, or precursor for the synthesis of advanced materials. In addition to hydrochar, the process generates a liquid phase containing water with dissolved organic compounds, such as organic acids and sugars, which can be utilized or appropriately treated. A gaseous phase is also produced, consisting mainly of carbon dioxide and traces of other volatile gases [16].

However, HTC faces certain challenges. Hydrochar is not stable in soil over the long term, fresh material can be phytotoxic, and the low cost of fossil coal makes HTC production costs less competitive. Despite these limitations, there is growing interest in research on this technology, especially because hydrochar is not only used as a fuel but also in the development of innovative materials, such as supercapacitors (energy storage devices) and electrode materials for applications in electric mobility [15,16].

1.3.4.   Hydrothermal Liquefaction

Hydrothermal liquefaction (HTL) has become increasingly popular in recent years as a sustainable alternative to traditional fossil fuel production. HTL is a thermochemical process that converts wet biomass into liquid, solid, and gaseous fractions by applying moderate temperatures and pressures under subcritical water conditions. In some cases, this method may involve the use of organic solvents or catalysts to enhance process efficiency. Typical temperatures range from 250 °C to 370 °C, while pressures reach levels between 4 and 22 MPa [17]. During the process, the feedstocks, usually wet, are combined with additional water in weight ratios of approximately 1:5, eliminating the need for prior drying, which is a key advantage of HTL [18].

As the process conditions approach the critical point of water (374 °C and 22 MPa), the physicochemical properties of water change significantly. These changes include variations in its density, dielectric constant, and permittivity. In this compressed state, water remains in the liquid

phase but exhibits unique characteristics: a higher ionic product and lower relative permittivity compared to normal conditions. These properties enable water to act as both a solvent and a chemical reactant, facilitating a series of transformations in the biomass [9].

One of water's key roles under these conditions is its ability to break down cell structures, disrupt metastable systems (those that appear stable but can easily be disturbed by changes in external conditions), and modify the sedimentation balances of biomass components.

The moderate pressure and temperature also reduce the density of water, weaken hydrogen bonds, and increase the solubility of nonpolar organic compounds. This, in turn, facilitates the decomposition of biopolymers-macromolecules like proteins, lipids, and carbohydrates found in living organisms [18].

Water, in its catalytic role, promotes the breakdown of complex molecules into simpler products. This leads to the formation of liquid fractions, such as biocrude and water-soluble compounds; gaseous fractions, composed of CO_2, CH_4, and other gases; as well as solid fractions. This set of reactions makes HTL an efficient and sustainable technology for utilizing wet biomass and transforming it into useful products, focusing on energy recovery and the production of value-added materials [2,9,18].

1.3.4.1. *Main chemical reaction pathways*

Due to the complexity of biomass, identifying all the reaction pathways leading to the formation of biocrude is a significant challenge. Some components of biocrude are derived directly from the raw materials, while others are generated through various chemical reactions, such as hydrolysis, depolymerization, decomposition, and recombination of reactive fragments. These transformations highlight the variety and intricacy of the chemical processes involved [2].

To better understand the reaction mechanisms in hydrothermal liquefaction (HTL), studies have been conducted using model compounds that simulate the main characteristics of biomass. Additionally, research has emphasized the role of key reactions, such as Maillard reactions, which

significantly influence biocrude formation by facilitating interactions between proteins and carbohydrates [19]. These interactions not only affect the final composition of the biocrude but also provide valuable knowledge for optimizing the process.

Figure 5 illustrates a general reaction network involved in the hydrothermal liquefaction (HTL) of sewage sludge, demonstrating how the primary chemical components of sludge, such as carbohydrates, proteins, and lipids, are transformed into various products (biocrude, aqueous phase, solid phase, and gases) under specific temperature conditions [9,19].
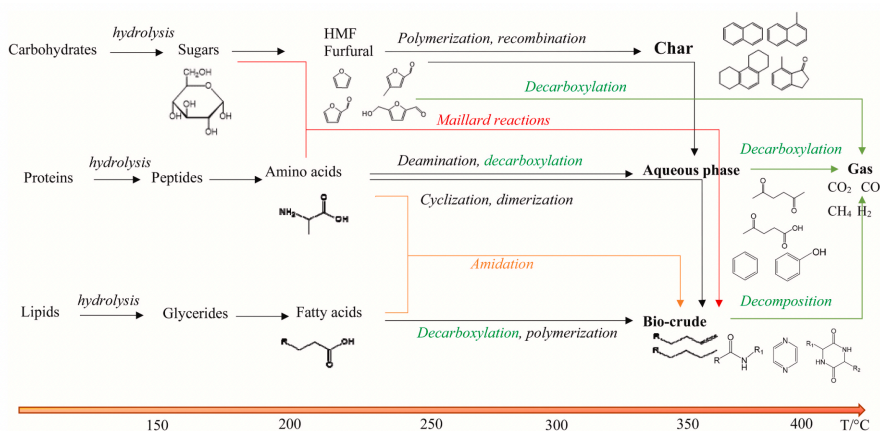
Figure 5. General reaction network in HTL of sewage sludge, showing the transformations of carbohydrates, proteins, and lipids into products such as bio-crude, char, aqueous phase, and gases under different temperatures *(extracted from [9])*.

1.3.4.2. Carbohydrates reaction

First of all, carbohydrates go through hydrolysis, breaking down into simple sugars such as glucose (r1) [20,21].

$$(C_6H_{10}O_5)_n + nH_2O \rightarrow nC_6H_{12}O_6 \quad (r1)$$
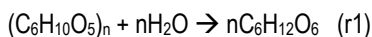
These sugars are then transformed into soluble intermediates such as 5-hydroxymethylfurfural (HMF) and furfural (r2).

$$C_6H_{12}O_6 \rightarrow C_6H_6O_3 + C_5H_4O_2 + H_2O + CO_2 \quad (r2)$$
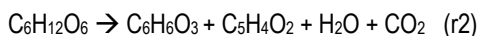
The latter can undergo polymerization and recombination to form char or decarboxylation reactions that release gases like carbon dioxide (r3).

$$C_6H_6O_3 \rightarrow Char + CO_2 \quad (r3)$$

Additionally, interactions between carbohydrates and proteins, known as Maillard reactions, can inhibit the carbonization of sugars and enhance bio-crude formation, highlighting the complexity of chemical interactions in the process (r4) [20,21].

$$C_6H_{12}O_6 + R - NH_2 \rightarrow Products \rightarrow Bio\text{-}crude \quad (r4)$$

1.3.4.3. Protein

Proteins, on the other hand, decompose through hydrolysis into peptides and amino acids (r5).

$$(Protein)\ R - CO - NH - R_2 + H_2O \rightarrow R - COOH + R_2 - NH_2 \quad (r5)$$
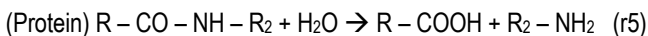
These products can undergo deamination, releasing ammonia (NH_3) (r6), and decarboxylation, generating carbon dioxide (CO_2) (r7).

$$R - CHNH_2COOH \rightarrow R - COOH + NH_3 \quad (r6)$$
$$R - CHNH_2COOH \rightarrow R - CHNH_2 + CO_2 \quad (r7)$$

These reactions contribute to the formation of compounds in the aqueous phase, while secondary processes such as cyclization and dimerization contribute to both biocrude and aqueous phase products. Maillard reactions also play a significant role by modifying the distribution of final products through their interaction with carbohydrates [22].

1.3.4.4. Lipids

Lipids initially transform through hydrolysis into glycerides and fatty acids (r8).

$$(C_{17}H_{35}COO)_3C_3H_5 + 3H_2O \rightarrow C_3H_8O_3 + R - COOH \quad (r8)$$
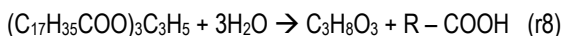
Fatty acids can subsequently undergo decarboxylation and polymerization, significantly contributing to bio-crude formation (r9) [21].

$$R - COOH + 3H_2O \rightarrow R - H + CO_2 \quad (r9)$$
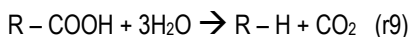
At higher temperatures, lipids can undergo thermal cracking, facilitating the production of gases such as methane (CH_4) and hydrogen (H_2) [21].

1.3.4.5. Reactions products

The aqueous phase is characterized by water-soluble organics compounds, such as amino acids, organic acids, and polar molecules, which result from initial decomposition reactions. Secondary reactions like condensation, recombination, and repolymerization can also contribute to the formation of biocrude or char. Meanwhile, the gaseous phase, composed of gases such as CO_2, CO, CH_2, and H_2, results from reactions such as decarboxylation, deamination, and the thermal cracking of lipids into light hydrocarbons [22,23,24].

The solid phase, or char, is primarily generated through the polymerization and recombination of large organic fragments such as HMF, with the carbonization of carbohydrates being a key contribution to its formation [22].

In this context, it is also essential to consider the behavior of ash present in sewage sludge at the beginning of the process. Ash represents the non-combustible inorganic fraction, composed of minerals such as silicon, calcium, iron, and aluminum oxides, among others. During HTL, ash does not participate in chemical reactions, as it is inert, and it primarily concentrates in the solid fraction (char) at the end of the process [24]. Although it does not contribute to the conversion of organic matter into biocrude, gas, or the aqueous phase, ash can inhibit process efficiency by increasing the amount of solid residues requiring post-process management. However, it may contain valuable trace metals that could be recovered, though their safe reuse may be limited by the presence of toxic heavy metals [24].

1.3.4.6. Temperature effect

Temperature is one of the most critical factors in hydrothermal liquefaction (HTL), as it plays a crucial role in chemical reactions and the distribution of the generated products. According to the literature, HTL temperatures range from 150 to 450 °C, and higher temperatures significantly enhance processes such as the hydrolysis of organic compounds [24,25].

Figure 5 illustrates how reactions are distributed across a temperature range of 150 to 400°C. At low temperatures (150–250 °C), hydrolysis and the formation of intermediates predominate; at intermediate temperatures (250–350 °C), processes such as deamination, decarboxylation, and condensation intensify, favoring the production of biocrude and aqueous compounds. Meanwhile, at high temperatures (>350 °C), secondary reactions such as thermal cracking and repolymerization prevail, increasing the generation of gases and solids (char). This temperature range highlights how HTL optimizes the transformation of sludge components into valuable products under different process conditions [24,25,26].

2. OBJECTIVES

Given the variability in sludge composition and the complexity of the chemical reactions involved, developing precise models for process optimization is challenging. Nevertheless, the main objective of this project is to develop a rigorous process simulation model, based on experimental data, for the hydrothermal liquefaction (HTL) of sewage sludge, with the aim of making accurate predictions about product yields.

In this context, the following specific objectives were proposed:

1. Characterize the composition of sewage sludge derived from wastewater, in this case the wastewater sludge used was collected from a wastewater treatment plant in Rome, located in central Italy, managed by ACEA (Azienda Comunale Energia e Ambiente).
2. Obtain experimental data from the hydrothermal liquefaction process, with the goal of developing a kinetic model that accurately describes the chemical reactions involved.
3. Validate the kinetic model studied by using material balances expressed through differential equations.
4. Develop a simulation model to optimize the operating conditions of the hydrothermal liquefaction process.

3. HYPOTHESES

Two models were developed for this study: (a) a kinetic model at the laboratory scale, validated with experimental data obtained under laboratory conditions, and (b) a scaled model representing the implementation of hydrothermal liquefaction (HTL) in a wastewater treatment plant.

The second process model was built using Aspen Plus v12, and the following general assumptions were applied:

- The processes are simulated in a steady-state mode.

- Each reaction pathway follows first order kinetics and adheres to the Arrhenius equation.

- The process feedstock (sewage sludge) and the generated products (biocrude, water-soluble organics, solid residues, and gases) are represented as non-conventional compounds, as they lack a fixed or standardized chemical composition due to their complex and heterogeneous nature.

- It is assumed that the kinetic model used are applicable to both primary and secondary sewage sludge.

Regarding the expected results at the end of the experiments:

- As the temperature increases, a higher conversion of organic matter in the sludge into liquid (biocrude) and gaseous products is anticipated due to the intensification of thermochemical reactions.

- Initially, the process will be dominated by the initial decomposition of macromolecules (such as lipids, proteins, and carbohydrates). After that, the formation of secondary products and rearrangement reactions are expected to prevail.

- The biocrude yield will increase with temperature, reaching a maximum within an intermediate time range, as longer times may promote its degradation into gaseous and aqueous products.

- At lower temperatures, less biocrude is likely to be generated due to the incomplete decomposition of organic matter.

- Lower temperatures are also expected to result in a considerable fraction of solid residues, as the thermal energy will not be sufficient to fully break down the organic molecules present in the sludge. This implies that a significant portion of organic or inorganic matter will remain unconverted into biocrude, gases, or water-soluble compounds.

4. MATERIALS AND METHODS

4.1.   MATERIALS:

4.1.1.   Sewage Sludge

The primary sludge from wastewater was obtained from a wastewater treatment plant operated by ACEA in Rome, Italy, and was used as received. Its chemical characteristics are presented in Table 1.

Table 1. Chemical characteristics of the sludge.

Moisture content as received (%wt)	Elemental analysis (%wt)					Ashes (%wt)	HHV (MJ/kg)
	C	H	N	S	O		
75,6	33,2	4,00	5,70	1,10	17,1	37,1	23,7

The HHV (Higher Heating Value) was determined using the formula [27]: HHV (MJ/kg) = 0.3383C + 1.443 (H-O/8) + 0.0927S.

Moreover, Table 2 provides the compound composition of the sewage sludge in terms of weight percentage (%wt).

Table 2. Compound composition of the sludge.

Compounds composition of sewage sludge (%wt)			
Lipids	Carbohidrates	Protein	Ashes
21,6	5,7	35,6	37,1

The protein content was calculated by multiplying the nitrogen percentage by 6.25 [28], the lipid content was determined using HTL and Soxhlet extraction with methanol and hexane, and the carbohydrate percentage was obtained by difference.

4.1.2.   Solvents properties

Table I to III show the characteristics of the solvents (Appendix I).

4.2.   EXPERIMENTAL PROCEDURE:

This section provides a detailed description of the procedures performed for the hydrothermal liquefaction (HTL) of sewage sludge, covering reactor preparation, reaction processes, product separation and filtration, and product extraction and analysis (Figure 6). It is divided into four main phases: reactor preparation, reaction process, separation and filtration, and extraction and analysis of the obtained products. The process is repeated three times for each specified time and temperature.
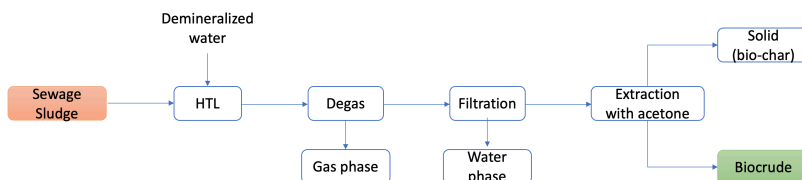
Figure 6. Flow diagram of the HTL process to obtain biocrude, biochar, and aqueous and gas phases from sewage sludge.

4.2.1.   Reactor Preparation

The preparation of the reactors is a fundamental step to ensure the safety of the experiment and the accuracy in measuring the quantities of reactants. Cylindrical reactors with a 10 mL capacity (1.13 cm in diameter and 12.7 cm in length) are used due to their ability to withstand the high pressures and temperatures required in the process.

Procedure:

1. Ten milliliter batch reactors are used, with their caps wrapped in tape to prevent leakage during the experiment.

2. Each reactor is weighed along with the caps and tape using a high precision analytical balance.

3. One gram of sewage sludge provided by ENEA and five grams of demineralized water are added to the reactor.

4. Once both reactants are added, the reactor is carefully sealed and weighed to record its starting mass before beginning the experiment.

4.2.2. Reaction Process

The hydrothermal liquefaction reaction is conducted in a fluidized sand bath at controlled temperatures. It is essential to stabilize the temperature before starting the effective reaction time to ensure homogeneous conditions inside the reactor.

Procedure:

1. The reactors are placed in a sand bath set to temperatures of 280°C, 300°C, or 320°C, with constant agitation at 140 rpm (Figure 7).

   Note: The agitation speed prevents the caps from separating due to centrifugal force and ensures a homogeneous reaction.

2. A three-minute stabilization period is allowed before starting the reaction time to stabilize the reactor temperature. This period is not considered part of the effective reaction time, as the chemical reactions characteristic of HTL depend on reaching and maintaining the desired temperature at a constant level.

3. Once the temperature is stabilized, the reaction time is timed (ranging from 0 to 30 minutes, depending on the experimental conditions).

4. At the end of the retention time, the reactors are removed from the sand bath and immersed in a water bath at room temperature to cool them quickly.
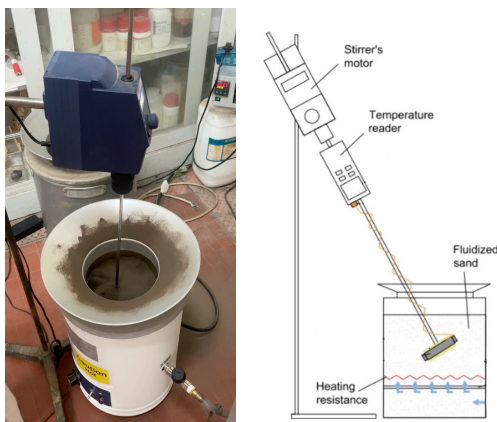
Figure 7. Experimental setup for hydrothermal liquefaction (HTL) using a sand bath and a stirring system.

4.2.3.   Gaseous Phase Separation and Filtration

After the reaction, the generated phases (liquid and gas) are separated using weighing and filtration techniques. This step is crucial to determine the distribution of the generated products.

4.2.3.1.   *Initial measurements*

1. The reactor, cooled to room temperature, is weighed to record the mass after the reaction.
2. A dry piece of paper is weighed to clean any residual liquid that may escape when the reactor is carefully opened. The wet paper is then weighed to calculate the amount of adhered liquid.
3. After 10 minutes with the reactor open, it is weighed again, and the difference between the closed and open reactor corresponds to the quantity of gas.

4.2.3.2.   *Aqueous phase separation*

1. An empty beaker is weighed to collect the aqueous phase.

2. An air pump is connected to the reactor to force the water out through filter paper. The reactor is placed upside down, with the filter paper at the bottom and the pump at the top (Figure 8a).

3. Once all the water has been extracted, the beaker containing the aqueous phase is weighed to determine its mass.

4. Additionally, a small amount (<1 g) of water is transferred to a watch glass and left to stand until the following day to evaporate the water and obtain the dissolved organic compounds (Figure 8b).
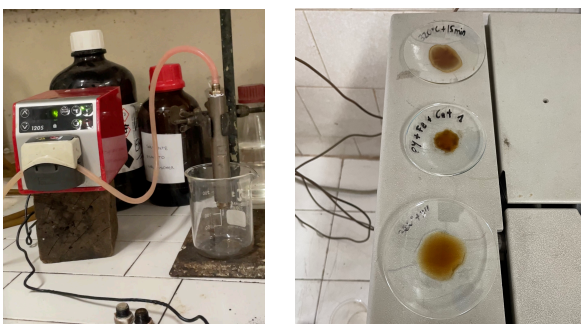
Figure 8. a) Experimental setup featuring an air pump utilized for the water filtration process; b) Organic solvents extracted from the aqueous phase.

4.2.4. Product Extraction and Analysis

The separation of solid products (char) and biocrude is performed using Soxhlet extraction. This process ensures an efficient separation of the solid and liquid phases for further analysis and quantification.

Procedure:

4.2.4.1. Preparation of the Soxhlet extractor

1. A cellulose thimble with a diameter of 10 mm is weighed along with cotton, both previously dried in an oven at 80°C to remove any moisture.

2. The solid content from the reactor is transferred to the thimble using a spatula. Both the thimble and the cotton, used earlier to clean the spatula, are included in the Soxhlet extractor.

4.2.4.2.   Assembly of the Soxhlet system

1. The thimble is inserted into the top section of the Soxhlet extractor.
2. At the bottom, a previously weighed empty distillation flask is attached, into which acetone is added as a solvent until three quarters full.
3. At the top of the Soxhlet extractor, a condenser is placed and cooled with water to condense the vaporized acetone.
4. The entire system is placed on a heating plate, which is adjusted to power 4, to initiate the extraction process (Figure 9).

Figure 9. Soxhlet system equipped with a condenser at the top and a heating plate at the bottom.

4.2.4.3. Bio-oil extraction

1. The Soxhlet system is operated for 24 hours. During this time, the acetone evaporates, condenses in the condenser, and returns to the thimble in liquid form, extracting the biocrude from the char.

2. Once the process is complete, the distillation flask contains both the acetone and the biocrude. This mixture is then processed using a rotary evaporation to separate the solvent from the biocrude (Figure 10).

Figure 10. Rotary evaporator used for the separation of acetone and bio-oil.

4.2.4.4. Quantification of biochar and bio-oil

1. The cellulose thimble is removed from the Soxhlet, dried in an oven at 80°C, and quickly weighed. The difference between the initial and final weight of the thimble corresponds to the mass of the char.

2. The biocrude in the distillation flask (after separated from acetone) is weighed. The difference between the weight of the empty flask and the final weight is recorded as the mass of the recovered biocrude.

4.3.   KINETIC MODEL VALIDATION:

The validation of the kinetic model under study was carried out using Microsoft Excel. For each reaction pathway, mass balances were applied, considering a first-order kinetics described by the Arrhenius equation. The associated differential equations were solved using the Euler method, a numerical tool that approximates solutions based on initial values and a specific integration step. The validation involved comparing experimental results with the values calculated by the model at 300ºC, thereby assessing its accuracy and consistency. Additionally, the model was also evaluated at other temperatures, specifically 250ºC, 350ºC, and 400ºC.

4.4. MODELIZATION OF THE HTL IN ASPEN PLUS V12:

This section provides a detailed description of the procedure carried out in Aspen Plus v12 to simulate the hydrothermal liquefaction (HTL) process of sewage sludge. The modelling focuses on the reaction stage, incorporating experimental parameters, operating conditions, and a sensitivity analysis to optimize the process.

4.4.1. Biomass Composition

According to the literature [29,30,35], organic residues are typically dominated by carbohydrates, which account for more than 50% by weight (mannose, galactose, cellobiose). However, in the specific case of sewage sludge, its composition shows distinct characteristics: carbohydrates constitute 5.7% by weight, while proteins, such as valine, tyrosine, leucine, and aspartic acid, represent 35.6% by weight. This is followed by lipids (linoleic, stearic, and palmitic acids) at 21.6% by weight and ashes at 37.1% by weight.

This variation reflects the heterogeneous nature of sewage sludge and its origin. However, due to the lack of specific information on the detailed chemical composition of the biomass, biocrude, aqueous phase, and gas, non-conventional components were used in the simulation. These components allow for the representation of complex materials without a precise structural definition, which is appropriate for sewage sludge and the products generated during the process.

Although the biomass was modelled as a non-conventional component, it was necessary to define all its physical and chemical properties, such as the carbon, hydrogen, oxygen, nitrogen, and ash content, as well as the calorific value and approximate fractions, based on the data presented in Table 1. These values were introduced into Aspen Plus v12 to ensure accurate and consistent modelling aligned with the available experimental data.

In the simulation, both the sewage sludge and the final products (biocrude, water-soluble organic, solid residues, and gas) were represented as non-conventional components, using the previously defined composition data to perform the mass and energy balances in Aspen Plus v12.

4.4.2. Thermodynamic Model Used in the Simulations

The selection of the thermodynamic model in the simulation of chemical processes is a fundamental aspect to ensure accurate and reliable results, as the quality of the outputs directly depends on the proper choice of the model.

In particular, it is crucial that the selected model accurately estimates thermodynamic properties and ensures the convergence of vapor-liquid equilibrium (VLE) calculations [32].

For the HTL conversion process, the SRK thermodynamic model was selected, based on the Soave-Redlich-Kwong cubic equation of state. This model is particularly suitable for conditions near the critical point of water, where solubilization of compounds and the decomposition of macromolecules are enhanced. In this simulation, the SRK-KD variant was applied, incorporating the Kabadi-Danner mixing rules to account for the immiscibility between hydrocarbons and water [32].

The SRK-KD model has been widely validated in the scientific literature and is recommended for applications in gas treatment, refineries, and petrochemical processes due to its ability to handle systems with complex phases and heterogeneous mixtures [32].

4.4.3. Simulation of the HTL Process

The hydrothermal liquefaction process was fully designed and simulated using Aspen Plus v12 software. This program enables the estimation of flow rates, compositions, and stream properties. Preliminary calculations of kinetic parameters were performed in Google Colab and subsequently implemented in Aspen Plus. Some physical parameters were obtained directly from available literature data, while others were derived from these data and optimized during the process.

According to previous studies, the HTL process can be divided into four main stages: pretreatment, reaction, separation, and upgrading [32]. In this work, the focus has been placed on the reaction stage, as it represents the core of the process where the transformation of biomass into target products occurs. Additionally, key parameters will be optimized through sensitivity analysis, comparing the results with those reported in the literature.

To perform the simulation, experimental data obtained from tests conducted in La Sapienza's laboratory were used. All unit operations included in the hydrothermal liquefaction process were modeled by applying fundamental principles, encompassing mass and energy balances as well as phase equilibrium.

4.4.3.1. Plant Capacity

The design of a hydrothermal liquefaction (HTL) plant depends on the daily waste flow it processes and the specific composition of the sludge. In this study, the wastewater sludge was sourced from a treatment plant in Rome, central Italy, managed by ACEA (Azienda Comunale Energia e Ambiente). The sample was provided through ENEA, the Italian National Agency for New Technologies, Energy, and Sustainable Economic Development.

The plant has been dimensioned with the capacity to process 50 kton/year of biomass, operating for 334 days per year, which corresponds to a flow rate of 6,240 kg/h of biomass and 31,200 kg/h of water.

This capacity was selected to ensure the technical and economic feasibility of the process. The recommendation that each treatment line should not exceed 15–18 t/h was taken as a reference, based on similar studies reported in the literature [33]. The defined plant size provides a balance between operational efficiency and investment costs.

4.4.3.2. Reaction stage

The reaction stage involves the conversion of biomass and water into biocrude, aqueous phase, solid residues, and gaseous products. The operating conditions were determined based on experimental data obtained from tests conducted in La Sapienza's laboratory, establishing the following parameters: a temperature of 300°C, a pressure of 210 bar, and a residence time of 25 minutes.

Under these conditions, water reaches almost supercritical state, which increases its ionic product and reduces its dielectric constant. These changes facilitate the breaking of hydrogen bonds, improve the solubility of nonpolar compounds, and promote the decomposition of biomass macromolecules into smaller organic molecules [32]. This environment enhances the chemical reactions necessary for the conversion of biomass into higher value products.

The reaction model was implemented in Aspen Plus using an RYield reactor, a tool that allows the simulation of the conversion of non-conventional components into specific products, and a separator. The final products generated include biocrude, aqueous phase, gas, and solid residues, thus representing a simplified version of the actual process. This configuration is suitable for systems where the precise reactions are not fully defined but still enables the execution of mass and energy balances to analyze the overall system behavior.
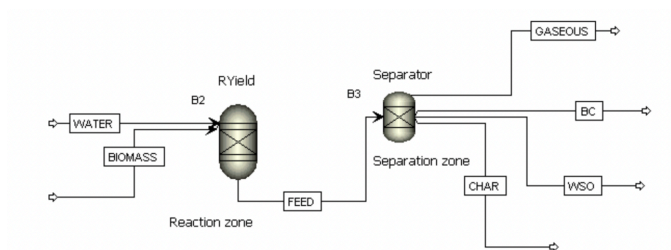
Figure 11. Schematic of the reaction model implemented in Aspen Plus using an RYield reactor and a separator for the conversion of biomass and water into biocrude, water-soluble organics, gas, and solid residues.

5. RESULTS AND DISCUSION

5.1. BIOCRUDE YIELD:

Based on the experimental data collected, Figure 12 illustrates the evolution of biocrude yield as a function of reaction time for three different temperatures (280 °C, 300 °C, and 320 °C) in the hydrothermal liquefaction process. Under all the conditions studied, the biocrude yield rises quickly the initial minutes of the reaction, reaching a peak before stabilizing or slightly decreasing. The temperature of 300 °C stands out for producing the highest yields, reaching approximately 30% at 20–25 minutes, suggesting that this condition is optimal for maximizing biocrude production. At 280 °C, although yields are consistent and stable, they are slightly below of 25%, the maximum observed at 300 °C. In contrast, at 320 °C, yields decrease to approximately 22% and show greater variability, potentially indicating that secondary reactions, such as gas formation or thermal decomposition of intermediate compounds, are more prominent at this temperature.

Reaction time also plays a crucial role in process efficiency. While the yield initially increases significantly, a saturation point is reached at all temperatures, beyond which longer reaction times do not contribute to additional biocrude production. This is particularly evident at 300 °C and 320 °C, where after 20–25 minutes, the values stabilize or even slightly decrease, possibly due to the decomposition of biocrude into other phases, such as gases or water-soluble compounds.

The variability in results, represented by error bars, is more notable under conditions with higher yields, such as at 300 °C and 25 minutes, suggesting a greater sensitivity of the chemical reactions to slight changes in experimental conditions. Additionally, fluctuations at 320 °C could be attributed to a higher incidence of undesirable secondary reactions, complicating the stability of biocrude yield.

Figure 12. Biocrude yields (% d.b.) obtained at different temperatures as a function of reaction time. Error bars represent standard deviations based on experimental replicates.

5.2.   SOLID RESIDUE YIELDS:

Figure 13 illustrates the evolution of solid residue yields as a function of reaction time for three different temperatures (280 °C, 300 °C, and 320 °C) in the hydrothermal liquefaction process. This analysis evaluates how the remaining solids in the system vary under different temperature and time conditions, providing key insights into the efficiency of solid conversion into biocrude, gases, or water-soluble compounds.

At 320 °C, the solid residue yield is the highest, reaching between 45% and 50%, and remains almost constant throughout the reaction time, with slight variations around 30 minutes. This increase in the percentage of solid residues may be attributed to part of the biocrude or aqueous phase being converted into char under these conditions, rather than transforming into other phases. At this temperature, secondary reactions such as thermal cracking and repolymerization prevail, further increasing char generation.

At 300 °C, solid residue yields start slightly lower, around 40% to 42%, and gradually decline over the first 25 minutes. This trend suggests that a larger fraction of the solids is converted into biocrude or water-soluble compounds at this temperature.

At 280 °C, solid residues start with the lowest initial values, around 38 to 40 percent, and show a noticeable decrease over the reaction time. However, this decrease is not as significant as at 300 °C, as hydrolysis and the formation of intermediates predominate at this temperature. The thermal energy is insufficient to fully convert these intermediates into biocrude or water-soluble organics.

Reaction time plays a critical role in the conversion of solids. At 320 °C, the solid yield remains almost unchanged, whereas at 280 °C and 300 °C, a steady decrease is observed over time. This decline reflects the gradual transformation of solids into liquid or gaseous products. These observations highlight how temperature and reaction time together influence the efficiency of the process.

Regarding experimental variability, the error bars demonstrate relative consistency in the results, particularly at 320 °C, indicating that reactions associated with solids are more predictable under these conditions.
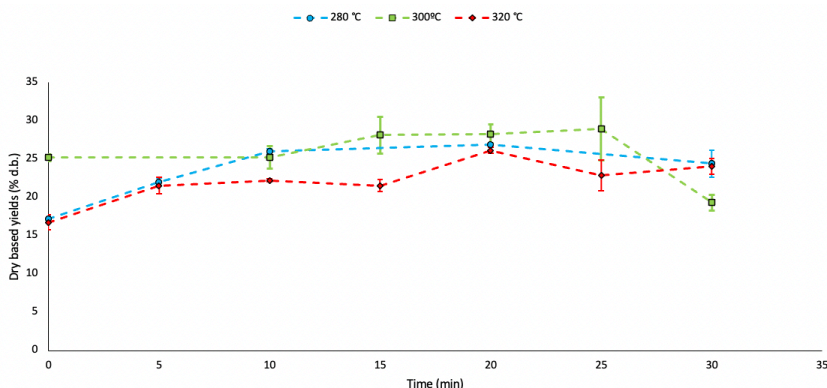

Figure 13. Solid residue yields (% d.b.) at different reaction temperatures as a function of reaction time. Error bars represent standard deviations based on experimental replicates.

5.3.   GASEOUS PHASE YIELDS:

Unlike the other phases analyzed, gaseous yields exhibit a more fluctuating and less stable evolution over time, depending on the temperature and process conditions.

At 280 °C, the gas phase starts with a relatively high yield of about 14% but quickly drops within the first 5 minutes, stabilizing at around 10–12% for most of the process. Toward the end of the reaction, at approximately 30 minutes, a slight increase is observed.

At 300 °C, gas yields start relatively low, around 9%, but gradually increase over time, peaking at nearly 15% after about 25 minutes. This suggests that this temperature supports steady gas production throughout the process, driven by decarboxylation and thermal cracking reactions of water-soluble compounds.

At 320 °C, the behavior is less consistent. Yields begin at around 12%, rise quickly within the first 10 minutes to a peak of 16%, then drop before increasing again near the end of the process, reaching about 15% at the 30 minute mark. This pattern indicates that higher temperatures encourage rapid gas formation but also lead to its consumption in secondary reactions or reflect some instability in the experimental setup. Moreover, the error bars highlight a more pronounced sensitivity in the gas phase yields to variations in the experimental conditions.
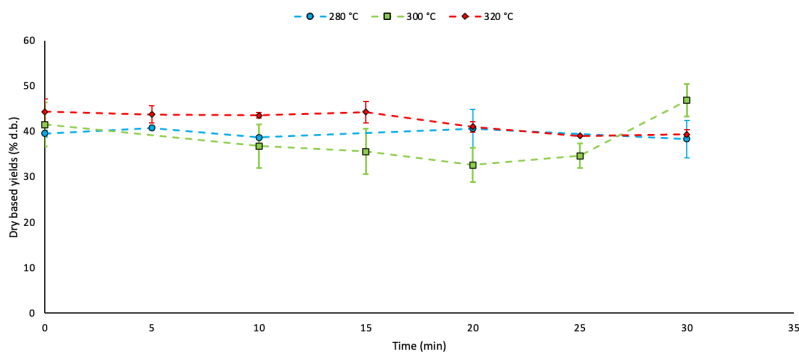
Figure 14. Gaseous phase yields (% d.b.) at different reaction temperatures as a function of reaction time. Error bars represent standard deviations based on experimental replicates.

5.4. WATER – SOLUBLE ORGANICS YIELDS:

Figure 15 shows the evolution of water-soluble organic compounds (WSO) yields which it changes over time during the hydrothermal liquefaction process at three different temperatures: 280 °C, 300 °C, and 320 °C. The analysis highlights the role of WSOs as intermediate products, which can further transform into gases depending on the reaction temperature and duration.

At 280 °C, the initial yields of water-soluble organic compounds, ranging from 20 to 25%, are the highest compared to the other temperatures. These values remain stable during the first 10 minutes, followed by a slight decrease between 20 and 30 minutes. This suggests that at lower temperatures, WSOs accumulate significantly, and their transformation into gases and biocrude occurs more slowly and gradually.

At 300 °C, WSO yields are lower, between 15 and 18%, showing a slight reduction around 15 minutes, followed by stabilization near 25 minutes. This behavior may indicate a dynamic balance where WSOs are produced and converted into the gas phase and biocrude more efficiently than at 280 °C.

At 320 °C, the yields are the lowest, between 12 and 15%, and decrease significantly during the first 15 minutes. Although a partial recovery is observed around 25 to 30 minutes, the values do not return to their initial levels. This pattern suggests that at higher temperatures, WSOs are rapidly converted into gaseous products, limiting their accumulation in the system.

Error bars highlight greater experimental variability at 280 °C, particularly around 10 to 15 minutes, possibly due to variations in the reactions generating WSO. At higher temperatures, variability decreases, reflecting a more uniform and controlled process.
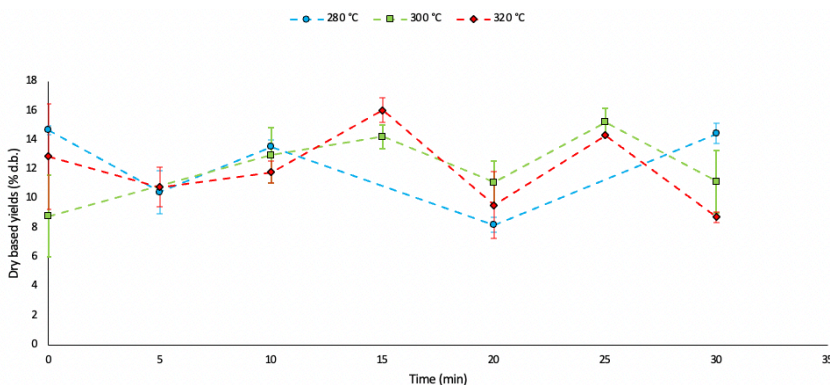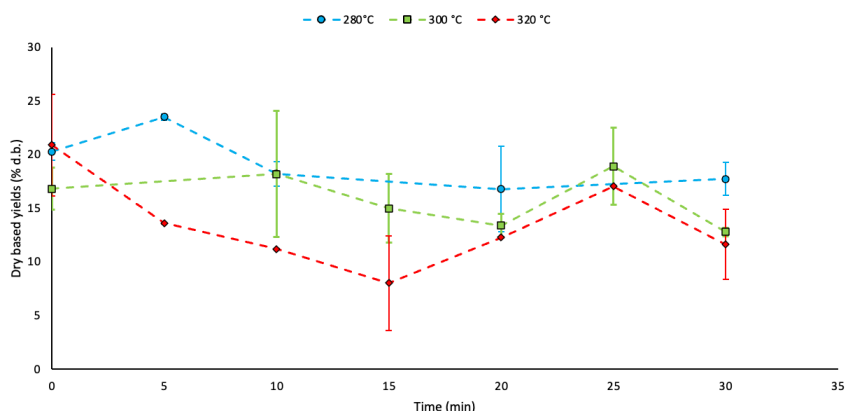

Figure 15. Water-soluble organic yields (% d.b.) at different reaction temperatures as a function of reaction time. Error bars represent standard deviations based on experimental replicates.

5.5. REACTION NETWORK:

The pathways considered in this study are depicted in Figure 16.

We employed the reaction network validated for the HTL process of *Nannochloropsis sp.* [33] and modified it. It is assumed that each reaction pathway in Figure 16 follows first order kinetics and adheres to the Arrhenius equation (Equation (1)):

$$k = Ae^{-\frac{E_a}{RT}}$$
(eq. 1)
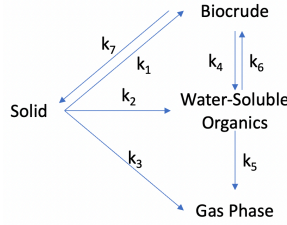
Figure 16. A reaction network for hydrothermal liquefaction of sludge.

Where the reaction rate constant (k) has units of s^{-1}. The term A is the pre-exponential factor, also with units of s^{-1}. E_a represents the activation energy required for the reaction to occur, expressed in J·mol^{-1}. The gas constant R is 8.314 J·mol^{-1}·K^{-1}. Finally, T is the absolute temperature of the system, measured in Kelvin.

The first order differential equations (Equations 2-5) mathematically describe the progress of the reactions in the batch reactors used in the experiment.

$$\frac{dY_{BC}}{dt} = k_1 Y_{SD} + k_6 Y_{AQ} - (k_4 + k_7)\, Y_{BC} \qquad \text{(eq. 2)}$$

$$\frac{dY_{AQ}}{dt} = k_2 Y_{SD} + k_4 Y_{BC} - (k_5 + k_1)\, Y_{AQ} \qquad \text{(eq. 3)}$$

$$\frac{dY_{SD}}{dt} = -(k_1 + k_2 + k_3)\, Y_{SD} + k_7\, Y_{BC} \qquad \text{(eq. 4)}$$

$$\frac{dY_G}{dt} = k_3 Y_{SD} + k_5 Y_{AQ} \qquad \text{(eq. 5)}$$

Where BC refers to biocrude; SD represents the residual solid; AQ corresponds to the aqueous phase; and G indicates the gaseous phase.

Google Colab was used to solve the differential equations and estimate the kinetic parameters from experimental data of the dependent variables Y_{BC}, Y_{AQ}, Y_{SD} and Y_G at different times. Cubic spline interpolation was applied to approximate the derivatives of the variables with respect to time and to reformulate the differential equations in terms of residuals. Then, the constants were fitted using numerical optimization by minimizing the squared error between the calculated derivatives and those predicted by the model. Finally, the constant values were obtained.

Table 3. Kinetic parameters estimated for the different reaction pathways of the hydrothermal liquefaction process at 300 °C.

Pathway	ln (A, [s^{-1}])	Ea [KJ/mol]	k(300ºC) [s^{-1}]
1. SD --> BC	12,5	78,1	0,020
2. SD --> WSO	13,80	86,3	0,013
3. SD --> G	6,20	91,0	2,51E-06
4. BC --> WSO	7,90	57,9	0,014
5. WSO --> G	14,4	99,6	0,002
6. WSO --> BC	14,1	89,1	0,010
7. BC --> SD	9,31	63,9	0,016

Table 3 summarizes the Arrhenius parameters for the reaction network shown in Figure 16. It also presents the reaction rate constants at 300 °C obtained in this study. The activation energy for the conversion of biocrude to aqueous phase products is the lowest (57.9 kJ·mol^{-1}), whereas the activation energy for the gasification of aqueous phase products was the highest one (99.6 kJ·mol^{-1}). Sheehan and Savage [33] reported that the activation energy for gas formation from aqueous phase products derived from protein HTL was 125 kJ·mol^{-1}, which is comparable to the result obtained in this study.

The biocrude yield initially increases with time and temperature, reaching a peak before stabilizing or slightly declining. This behavior is associated with the SD → BC pathway, which is characterized by a moderate activation energy of 78.1 kJ·mol^{-1} and a relatively high kinetic constant (k = 0.020 s^{-1} at 300 °C). At higher temperatures, biocrude tends to partially decompose into water-soluble organics, which can subsequently convert into the gas phase.

Solid residues exhibit a decreasing trend with increasing temperature, reflecting the gradual conversion of solids into biocrude, aqueous, and gaseous phases. The SD → WSO pathway is characterized by a moderate activation energy of 86.3 kJ·mol^{-1} and a moderate kinetic constant of 0.013 s^{-1}, favoring the formation of water-soluble compounds at the expense of the solid phase.

Regarding the water-soluble organics, their behavior also depends on the temperature. At 280°C, yields remain relatively constant, whereas at 300°C and 320°C, an initial increase followed by a decrease is observed. This reflects a balance between the formation (SD → WSO) and decomposition pathways towards biocrude or gas.

The gaseous phase steadily increases with both temperature and time, though its production remains limited due to the high activation energy required for the SD → G and WSO → G pathways, measured at 91.0 kJ·mol^{-1} and 99.6 kJ·mol^{-1}, respectively, combined with low kinetic constants of 0.002 s^{-1}.

Overall, the system achieves maximum biocrude yield at intermediate temperatures around 300 °C and reaction times, while 320 °C encourage the production of gaseous phases at the expense of liquids and solids. This indicates that 300 °C is closer to the optimal temperature for maximizing biocrude production.

5.6.   RESULTS OF THE KINETIC MODEL VALIDATION:

The validation of the kinetic model under study was conducted using Microsoft Excel, with the mass balances for each yield defined by equations 2-5. Figure 17 presents the fractional yields of products calculated during the HTL of sludge at reference temperatures of 250 ºC, 300 ºC, 350 ºC, and 400 ºC. The comparison of biocrude yields between experimental and calculated data at 300 ºC, shown in Figure 18, validates the kinetic model's ability to predict and optimize the performance of the HTL process. This minimizes the need for physical experimentation and allows for the estimation of data at temperatures beyond those tested in the laboratory.

Overall, the reaction network displayed in Figures 17 and 18, along with the Arrhenius parameters presented in Table 3, aligns well with the experimental data and their temporal variations. At 250 ℃, biomass conversion is slow, and the biocrude yield reaches a late maximum. At 300 ℃, the biocrude yield peaks around 25 minutes, followed by a slight decrease due to secondary reactions, confirming this temperature as optimal for maximizing yield. At 350 ℃, the biocrude yield reaches an early maximum but decreases rapidly due to the formation of aqueous and gaseous phases, a trend accurately captured by the model. Finally, at 400 ℃, solid conversion is nearly complete within a few minutes, but the biocrude yield is very low due to its rapid transformation into aqueous phases and subsequently into gaseous phase.
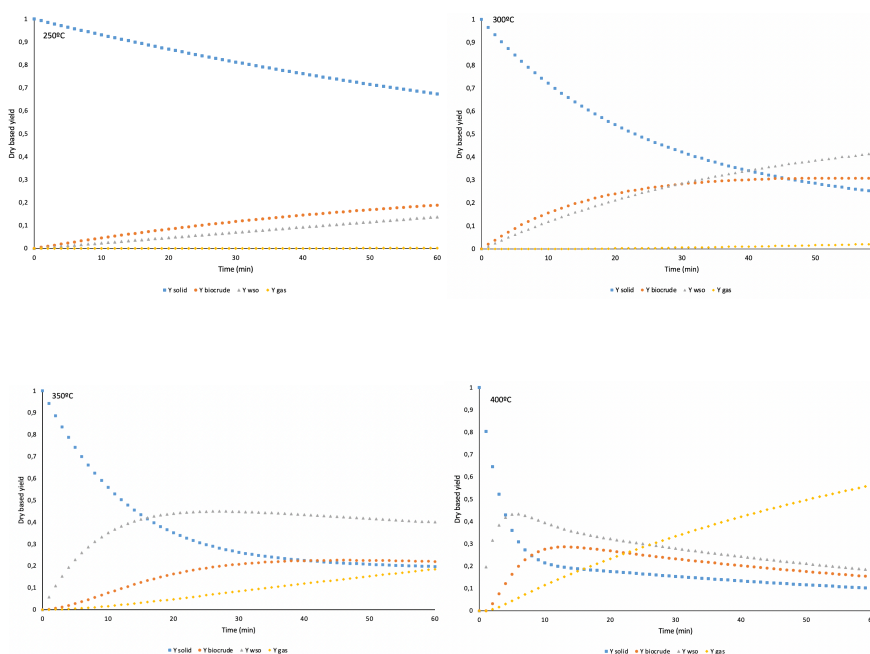
Figure 17. Calculated yields from hydrothermal liquefaction of sludge at set-point temperatures of:

(a) 250 °C; (b) 300 °C; (c) 350 °C; (d) 400 °C.
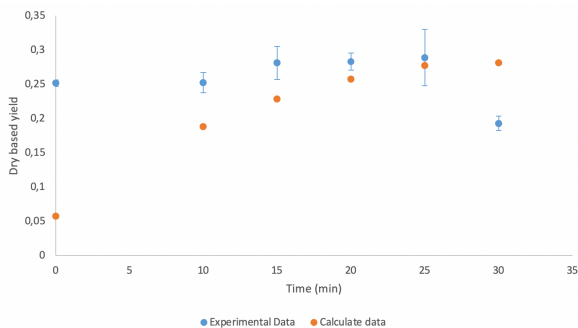
Figure 18. Comparison between calculated and experimental yields of biocrude at 300ºC.

At 300°C, significant discrepancies are observed between the calculated and experimental values for solid residues, water-soluble compounds, and the gas phase.

Regarding solid residues, in Figure 19, the model predicts a continuous decrease over time, indicating progressive biomass conversion. However, experimental data show that this decrease occurs only during the first 20 minutes, stabilizing thereafter. This suggests limitations in total conversion under the experimental conditions, possibly due to the formation of products not accounted for by the model.
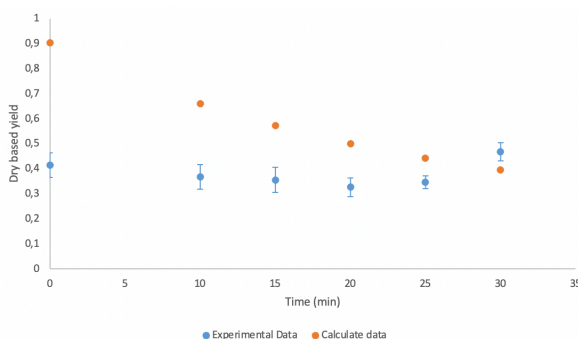
Figure 19. Comparison between calculated and experimental yields of solid residue at 300ºC.

On the other hand, as shown in Figure 20, the calculated values for water-soluble compounds display a steady increase. In contrast, the experimental results reveal a different behavior: the WSO initially increase, reach a peak, and then decrease before stabilizing at lower values. This behavior could be explained by secondary reactions that convert water-soluble compounds into the solid phase.
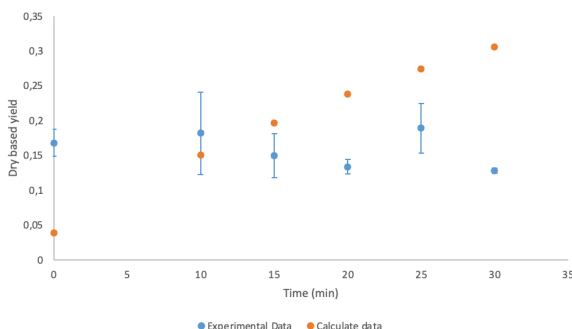
Figure 20. Comparison between calculated and experimental yields of WSO at 300ºC.

Finally, for the gas phase, the model predicts a steady increase over time, implying a constant generation of gases. However, experimental data reveal fluctuations in gas yields, even though the overall trend remains upward over longer periods. These variations could be influenced by factors such as changes in pressure, temperature, or interactions between the solid and liquid phases, all of which play a role in gas formation.

5.7.   RESULTS OF THE SIMULATION IN ASPEN PLUS:

Table XIII in the appendix 5 summarizes the mass flows (kg/h) of the products obtained at different reaction temperatures, ranging from 250 ºC to 400 ºC. The simulation results show that biocrude (BC) production is directly influenced by temperature. As the temperature increases, biocrude production rises, reaching a maximum of 2,897.6 kg/h at 300 ºC. Beyond this temperature, the yield begins to decrease, reflecting secondary decomposition processes and thermal cracking that promote gas formation. At 400 ºC, biocrude production decreases to 1,645.8

kg/h, while the gas flow significantly increases to 53.3 kg/h, indicating greater biomass conversion into the gas phase at higher temperatures.

Figure 21 shows the variation in biocrude yield with temperature, where a peak at 300 ºC is observed, suggesting that this is the optimal temperature for maximizing biocrude production.
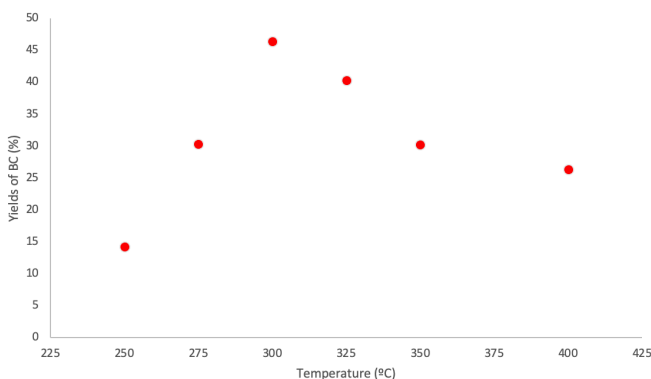
Figure 21. Results in biocrude yield depending on the temperature from the simulation in Aspen Plus.

The aqueous phase follows an upward trend with temperature, reaching its maximum value of 4,241.5 kg/h at 350 ºC, before experiencing a slight reduction at 400 ºC. This behavior is due to the thermal fragmentation of biomass components at intermediate temperatures, which favors the formation of water-soluble compounds. In contrast, the production of solid residues (char) shows a progressive decrease as the temperature increases, reflecting greater biomass conversion into liquid and gaseous phases.

The aqueous phase steadily increases with rising temperature, peaking at 4,241.5 kg/h at 350 ºC, before slightly decreasing at 400 ºC. This trend is likely due to the thermal breakdown of biomass components at moderate temperatures. On the other hand, the production of solid residues (char) gradually declines as temperature rises, indicating a more efficient conversion of biomass into liquid and gas phases.

The results suggest that 300 ºC is the ideal temperature for maximizing biocrude production. At temperatures above this point, cracking and gasification processes intensify, reducing biocrude yield while increasing gas production.

Figure 22 provides a closer look at gas production during the HTL process as temperature changes. From 325 ºC onward, gas production grows significantly, signaling the start of thermal cracking reactions. By 400 ºC, gas flow reaches a high level, following an exponential trend. This suggests that at higher temperatures, the conversion of aqueous and solid phases into gaseous products accelerates, emphasizing a shift toward gasification as the temperature increases.
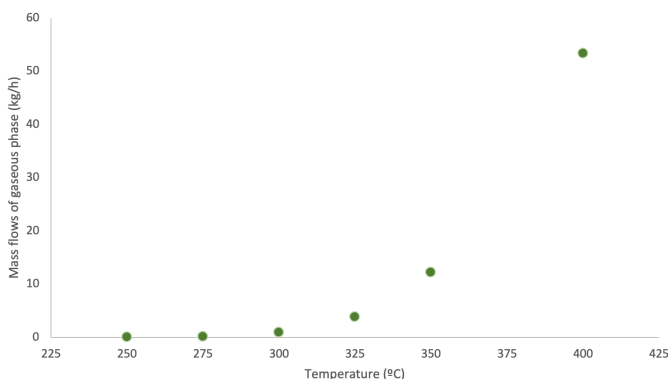
Figure 22. Gaseous phase production as a function of temperature from the simulation.

5.7.1. Comparison with Experimental Data

As mentioned earlier, Figure 21 once again highlights the variation in biocrude yield with temperature, showing a clear peak at 300 °C, confirming it as the optimal temperature. Similarly, Figure 12, which presents previous experimental data, shows a comparable trend, with maximum yields exceeding 30% on a dry basis (d.b.) around 300 °C. At temperatures of 320 °C or higher, the yield tends to decrease, following patterns equivalent to those observed in the simulation.

The overall consistency between the simulation results and the experimental data suggests that the reaction model implemented in Aspen Plus v12 accurately captures the system's behavior, validating its ability to predict biocrude yields. The simulation estimates a yield of approximately 46% on a dry basis, producing 2,897.6 kg/h of biocrude from 6,240 kg/h of biomass fed into the reactor. This result aligns well with the experimental values, reinforcing the reliability of the proposed model. However, some discrepancies remain, which are discussed in the following section.

5.7.2. Discussion of Discrepancies

The difference between the biocrude yield obtained in the simulation, 46.4 percent, and the experimental yield, 30 percent, at 300 ºC and with a residence time of 25 minutes, can be attributed to several factors that reflect the discrepancies between theoretical models and real operating conditions.

One of the main factors explaining this difference is the simplification of the simulation model. The use of an RYield reactor in Aspen Plus assumes ideal conversions, where biomass is directly transformed into biocrude, gas, aqueous phase, and solid residues, without considering the secondary reactions that occur under real conditions. In the experiment, as the temperature increases, it is common for a fraction of the biocrude to degrade into gas via pathway k8, as shown in Figure 23, reducing the final yield. This phenomenon, which is difficult to model accurately, may be one of the main reasons why the experimental yield is lower than that predicted by the simulation.
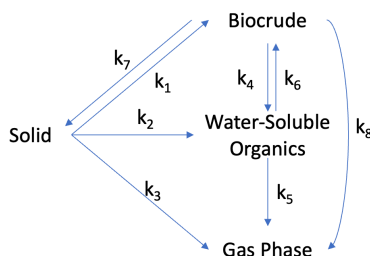
Figure 23. A possible reaction network for hydrothermal liquefaction of sludge.

Moreover, the simulation might overestimate the biocrude yield because it doesn't account for losses that typically occur during experiments. Factors such as inefficiencies in heat transfer, limited reactor mixing, and impurities in the biomass can negatively impact the yield. Additionally, during the separation and extraction of biocrude, there can be losses that the simulation doesn't capture. This is because simulations assume ideal conditions and don't consider biocrude trapped in the solids or dissolved in the aqueous phase.

Another important factor is the difference between the kinetic and thermodynamic models used in the simulation and how biomass behaves in real life conditions. Simulations often assume that reactions reach ideal equilibria based on fixed parameters, however, in experiments, reactions may remain incomplete due to variations in residence time, temperature, pressure, or the quality of the raw materials.

To reduce this gap, it's advisable to refine the simulation model by incorporating secondary reactions that better represent the thermal degradation processes of biocrude. Additionally, a detailed analysis of losses during the experiment could offer valuable insights and help narrow the discrepancies.

This comparison highlights the importance of integrating experimental data with simulation models, as it allows for the optimization of both operating conditions and reactor design, providing a more accurate understanding of the process.

6. CONCLUSIONS

This work has demonstrated that hydrothermal liquefaction (HTL) is a viable and promising technology for converting sewage sludge into biocrude and other useful products. By developing a kinetic model, validating it in Excel, and running simulations in Aspen Plus v12, the best conditions for maximizing biocrude production were identified: 300 ºC and a residence time of 25 minutes. Under these conditions, the biocrude yield was around 46% on a dry basis, which is consistent with experimental results of 30%.

The study also provided insights into how sludge components transform during the process. At higher temperatures, above 325 ºC, thermal cracking and gasification play a bigger role, with gas production increasing significantly at 400 ºC. Differences between the simulations and experiments are due to simplifications in the model, inefficiencies during the process, and variations in reaction conditions like temperature and pressure. Improving the model by adding secondary reactions could make predictions more accurate.

The designed HTL plant is an efficient and sustainable solution. It can process 50,000 tons of dry biomass each year and produce about 23,000 tons of biocrude. This makes HTL a cost-effective option for waste management and resource recovery. The results show that HTL can convert waste into valuable products and support a circular economy. However, its technical complexity is still a challenge, and more research is needed to improve its efficiency.

To sum up, this study advances the development of HTL as a technology for turning urban waste into biocrude, which can later be refined into biofuels. Hydrothermal liquefaction is not only a sustainable way to manage sludge but also a way to recover renewable energy. These findings provide a solid starting point for future research and bring this technology closer to being used on an industrial scale, contributing to a cleaner and more sustainable future.

REFERENCES AND NOTES

1. Buta, M.; Hubeny, J.; Zieliński, W.; Harnisz, M.; Korzeniewska, E. Sewage sludge in agriculture – the effects of selected chemical pollutants and emerging genetic resistance determinants on the quality of soil and crops – a review. Ecotoxicol. Environ. Saf. 2021, 214, 112116. DOI: 10.1016/j.ecoenv.2021.112070.
    https://www.sciencedirect.com/science/article/pii/S0147651321001810?via%3Dihub
2. Bagheri, M.; Bauer, T.; Burgman, L. E.; Wetterlund, E. Fifty years of sewage sludge management research: Mapping researchers' motivations and concerns. Resour. Conserv. Recycl., 2023, 191, 106899. DOI: 10.1016/j.resconrec.2022.106899.
    https://www.sciencedirect.com/science/article/pii/S0301479722019855?via%3Dihub
3. Oladejo, J.; Shi, K.; Luo, X.; Yang, G.; Wu, T. A Review of Sludge-to-Energy Recovery Methods. Energies 2019, 12, 60. DOI: 10.3390/en12010060. https://www.mdpi.com/1996-1073/12/1/60
4. Donatello, S.; Cheeseman, C. R. Recycling and recovery routes for incinerated sewage sludge ash (ISSA): A review. Waste Management 2013, 33, 2328–2340. DOI: 10.1016/j.wasman.2013.05.024.
    https://www.sciencedirect.com/science/article/abs/pii/S0956053X13002559
5. Wu, Y.; Wang, K.; He, C.; Wang, Z.; Ren, N.; Tian, Y. Effects of bioleaching pretreatment on nitrous oxide emission-related functional genes in sludge composting process. Bioresource Technology 2018, 249, 364–371. DOI: 10.1016/j.biortech.2017.10.008.
    https://www.sciencedirect.com/science/article/abs/pii/S0960852418308289
6. Zhou, K.; Barjenbruch, M.; Kabbe, C.; Inial, G.; Remy, C. Phosphorus recovery from municipal and fertilizer wastewater: China's potential and perspective. Journal of Environmental Sciences 2017, 52, 151–159. DOI: 10.1016/j.jes.2016.04.010.
    https://www.sciencedirect.com/science/article/abs/pii/S100107421630119X
7. Grifoni, M.; Pedron, F.; Rosellini, I.; Petruzzelli, G. 26 - From waste to resource: Sorption properties of biological and industrial sludge. Industrial and Municipal Sludge: Emerging Concerns and Scope for Resource Recovery 2019, 595–621. DOI: 10.1016/B978-0-12-815907-1.00026-X.
    https://www.sciencedirect.com/science/article/abs/pii/B978012815907100026X
8. Przydatek, G.; Wota, A. K. Analysis of the comprehensive management of sewage sludge in Poland. Journal of Material Cycles and Waste Management 2020, 22, 80–88. DOI: 10.1007/s10163-019-00928-z. https://link.springer.com/article/10.1007/s10163-019-00937-y
9. Fan, Y.; Hornung, U.; Dahmen, N. Hydrothermal liquefaction of sewage sludge for biofuel application: A review on fundamentals, current challenges and strategies. Biomass and Bioenergy 2022, 165, 106570. DOI: 10.1016/j.biombioe.2022.106570.
    https://www.sciencedirect.com/science/article/pii/S096195342200232X
10. Telwesa. Strategies for the Management of Sewage Sludge. Telwesa. Available online: https://telwesa.com/estrategias-gestion-de-lodos-residuales/ (accessed on 10th October 2024).
11. Fytilli, D.; Zabaniotou, A. Utilization of sewage sludge in EU application of old and new methods—A review. Renewable and Sustainable Energy Reviews 2008, 12, 116–140. DOI: 10.1016/j.rser.2006.05.014.
    https://www.sciencedirect.com/science/article/abs/pii/S1364032106000827

12.   Ecoembes. Pyrolysis of waste: What is it and what are its benefits? Available online (accessed on 13th October, 2024).: https://reducereutilizarecicla.org/pirolisis-de-residuos/#:~:text=La%20pir%C3%B3lisis%20es%20un%20procedimiento,pir%C3%B3lisis%2C%20biochar%20o%20algunos%20gases

13.   Zhu, F.; Zhao, L.; Jiang, H.; Zhang, Z.; Xiong, Y.; Qi, J.; Wang, J. Comparison of the Lipid Content and Biodiesel Production from Municipal Sludge Using Three Extraction Methods. Energy & Fuels 2014, 28, 8, 4752–4758. DOI: 10.1021/ef501054t. https://pubs.acs.org/doi/10.1021/ef500730c

14.   SCWG (Supercritical Water Gasification), CADE Soluciones de Ingeniería, S.L. Hydrothermal Gasification: Applications and Integration. Available online (accessed on October 28th, 2024): https://scwg.es/gasificacion-hidrotermal-aplicaciones-e-integracion/

15.   Wang, C.; Fan, Y.; Hornung, U.; Zhu, W.; Dahmen, N. Char and tar formation during hydrothermal treatment of sewage sludge in subcritical and supercritical water: Effect of organic matter composition and experiments with model compounds. Journal of Cleaner Production 2020, 242, 118586. DOI: 10.1016/j.jclepro.2019.118586. https://www.sciencedirect.com/science/article/abs/pii/S0959652619334560

16.   Heidari, M.; Dutta, A.; Acharya, B.; Mahmud, S. A review of the current knowledge and challenges of hydrothermal carbonization for biomass conversion. Journal of the Energy Institute 2019, 92, 1779–1799. DOI: 10.1016/j.joei.2018.12.003. https://www.sciencedirect.com/science/article/abs/pii/S1743967118306421

17.   Rodriguez Correa, C.; Kruse, A. Biobased Functional Carbon Materials: Production, Characterization, and Applications—A Review. Materials 2018, 11, 1568. DOI: 10.3390/ma11091568. https://www.mdpi.com/1996-1944/11/9/1568

18.   Gollakota, A.R.K.; Kishore, N.; Gu, S. A review on hydrothermal liquefaction of biomass. Renewable and Sustainable Energy Reviews 2018, 81, 1378–1392. DOI: 10.1016/j.rser.2017.05.178. https://www.sciencedirect.com/science/article/pii/S1364032117308146

19.   Su, Y.; Liu, D.; Gong, M.; Zhu, W.; Yu, Y.; Gu, H. Investigation on the decomposition of chemical compositions during hydrothermal conversion of dewatered sewage sludge. International Journal of Hydrogen Energy 2019, 44, 26933–26942. DOI: 10.1016/j.ijhydene.2019.08.182. https://www.sciencedirect.com/science/article/abs/pii/S0360319919332008

20.   Mo, N.; Savage, P. E. Hydrothermal Catalytic Cracking of Fatty Acids with HZSM-5. ACS Sustainable Chemistry & Engineering 2013, 2, 1–11. DOI: 10.1021/sc4003152. https://pubs.acs.org/doi/full/10.1021/sc400368n

21.   Peterson, A. A.; Lachance, R. P.; Tester, J. W. Kinetic Evidence of the Maillard Reaction in Hydrothermal Biomass Processing: Glucose–Glycine Interactions in High-Temperature, High-Pressure Water. Industrial & Engineering Chemistry Research 2010, 49, 2107–2117. DOI: 10.1021/ie9012433. https://pubs.acs.org/doi/10.1021/ie9014809

22.   Liu, X.; Zhu, F.; Zhang, R.; Zhao, L.; Qi, J. Recent progress on biodiesel production from municipal sewage sludge. Renewable and Sustainable Energy Reviews 2020, 119, 110260. DOI: 10.1016/j.rser.2020.110260. https://www.sciencedirect.com/science/article/abs/pii/S1364032120305499

23.   Fan, Y.; Hornung, U.; Dahmen, N. Hydrothermal liquefaction of sewage sludge for biofuel application: A review on fundamentals, current challenges and strategies. Biomass and Bioenergy 2022, 165, 106570. DOI: 10.1016/j.biombioe.2022.106570. https://www.sciencedirect.com/science/article/pii/S096195342200232X

24.   Qian, L.; Wang, S.; Savage, P. E. Fast and isothermal hydrothermal liquefaction of sludge at different severities: Reaction products, pathways, and kinetics. Applied Energy 2020, 260, 114312. DOI: 10.1016/j.apenergy.2019.114312. https://www.sciencedirect.com/science/article/pii/S0306261919319993?via%3Dihub

25. Malins, K.; Kampars, V.; Brinks, J.; Neibolte, I.; Murnieks, R.; Kampare, R. Bio-oil from thermo-chemical hydro-liquefaction of wet sewage sludge. Bioresource Technology 2015, 187, 23–29. DOI: 10.1016/j.biortech.2015.03.093.
https://www.sciencedirect.com/science/article/abs/pii/S0960852415004253

26. Dimitriadis, A.; Bezergianni, S. Hydrothermal liquefaction of various biomass and waste feedstocks for biocrude production: A state of the art review. Renewable and Sustainable Energy Reviews 2017, 68, 113–125. DOI: 10.1016/j.rser.2016.09.120.
https://www.sciencedirect.com/science/article/abs/pii/S1364032116306347

27. Chen, J.; Ding, L.; Wang, P.; Zhang, W.; Li, J.; Mohamed, B. A.; Chen, J.; Leng, S.; Liu, T.; Leng, L.; Zhou, W. The Estimation of the Higher Heating Value of Biochar by Data-Driven Modeling. Journal of Renewable Materials 2022. DOI: 10.32604/jrm.2022.018625.
https://www.techscience.com/jrm/v10n6/46593/html

28. Binaghi, M. J.; Baroni, A.; Greco, C.; Ronayne de Ferrer, P. A.; Valencia, M. Estimación de proteína potencialmente utilizable en fórmulas infantiles de inicio para neonatos prematuros y de término. Archivos Latinoamericanos de Nutrición 2002, 52, 1.
https://ve.scielo.org/scielo.php?script=sci_arttext&pid=S0004-06222002000100006

29. Wei, Y.; Xu, D.; Xu, M.; Zheng, P.; Fan, L.; Leng, L.; Kapusta, K. Hydrothermal liquefaction of municipal sludge and its products applications. Science of The Total Environment 2024, 908, 168177. DOI: 10.1016/j.scitotenv.2023.168177.
https://www.sciencedirect.com/science/article/abs/pii/S0048969723068043

30. Campuzano, R.; González-Martínez, S. Characteristics of the organic fraction of municipal solid waste and methane production: A review. Waste Management 2016, 54, 3–12. DOI: 10.1016/j.wasman.2016.05.016.
https://www.sciencedirect.com/science/article/abs/pii/S0956053X16302483

31. Okoro, O.V.; Sun, Z. The characterisation of biochar and biocrude products of the hydrothermal liquefaction of raw digestate biomass. Biomass Conversion and Biorefinery 2020, 10(6), 2947–2961. DOI: 10.1007/s13399-020-00672-7. https://ouci.dntb.gov.ua/en/works/4L8jKPj4/

32. Segneri, V. Waste to Chemicals: Analisi Tecnico–Economica di un Processo HTL. Sapienza Università di Roma, Facoltà di Ingegneria Civile e Industriale, Dipartimento di Ingegneria Chimica Materiali e Ambiente.

33. Valdez, P.J.; Savage, P.E. A reaction network for the hydrothermal liquefaction of Nannochloropsis sp. Algal Research 2013, 2(4), 416–425. DOI: 10.1016/j.algal.2013.08.002.
https://www.sciencedirect.com/science/article/pii/S2211926413000842

34. Sheehan, J.D.; Savage, P.E. Products, pathways, and kinetics for the fast hydrothermal liquefaction of soy protein isolate. ACS Sustainable Chemistry & Engineering 2016, 4(12), 6828–6837. DOI: 10.1021/acssuschemeng.6b01806. https://pubs.acs.org/doi/10.1021/acssuschemeng.6b01857;

APPENDICES

APPENDIX 1: EXPERIMENTAL TABLE

I.I. Acetone

Table I. Acetone propierties.

Property	Value
Molecular Formula:	C_3H_6O
IUPAC Name:	Propan-2-one
Categorization Safety:	Ketone
Chemical Safety:	Flammable Irritant
Molecular Weight (g/mol):	58.08
Density (g/cm³)	0.791
CAS Number:	67-64-1
EC Number:	200-662-2
Solubility (mg/mL):	Miscible in water
pKa:	20 (weakly acidic in water)
log Kow:	-0.24
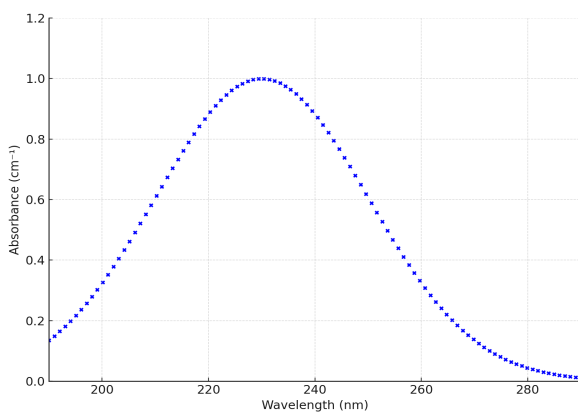
Figure I. Acetone absorption spectrum. Peak = 230 nm.

I.II. Methanol

Table II. Methanol propierties.

Property	Value
Molecular Formula:	CH_3OH
IUPAC Name:	Methanol
Categorization Safety:	Alcohol
Chemical Safety:	Flammable Toxic
Molecular Weight (g/mol):	32.04
Density (g/cm³)	0.791
CAS Number:	67-56-1
EC Number:	200-659-6
Solubility (mg/mL):	Miscible in water
pKa:	15.5
log Kow:	-0.77
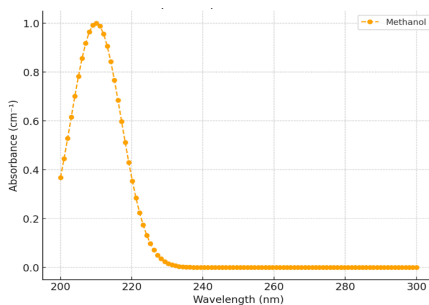
Figure II. Methanol absorption spectrum. Peak = 210 nm.

I.III. Hexane

Table III. Hexane propierties.

Property	Value
Molecular Formula:	C_6H_{14}
IUPAC Name:	Hexane
Categorization Safety:	Hydrocarbon
Chemical Safety:	Flammable Irritant
Molecular Weight (g/mol):	86.18
Density (g/cm³)	0.654
CAS Number:	110-54-3
EC Number:	203-777-6
Solubility (mg/mL):	Insoluble in water
log Kow:	3.9
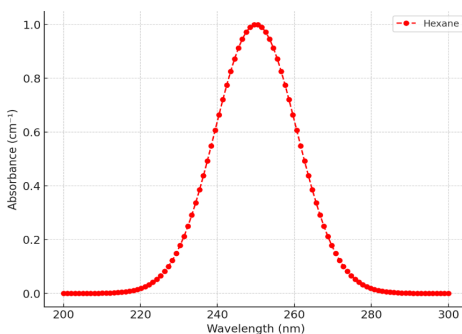
Figure III. Hexane absorption spectrum. Peak = 250 nm.

APPENDIX 2: EXPERIMENTAL TABLE

II.I. At 280ºC

Table IV. Summary of the experimental data obtained at 280°C.

	280ºC											
	A [3min+0min]	A [3min+0min]	D [3min+5min]	B [3min+5min]	D [3min+10min]	C [3min+10min]	C [3min+20min]	B [3min+20min]	C [3min+20min]	B [3min+30min]	D [3min+30min]	A [3min+30min]
	weight [g]	weight [g]	weight [g]	weight [g]	weight [g]	weight [g]	weight [g]	weight [g]	weight [g]	weight [g]	weight [g]	weight [g]
Reactor Empty	227,57	227,79	227,51	227,57	234,07	221,35	216,03	216,13	234,19	228,47	228,12	227,75
Biomass	1,0007	0,9999	1,0039	1,0037	0,9984	1,0023	0,9948	1,0006	0,9958	1,0095	1,0082	0,9997
Water	5,026	5,0189	4,9969	4,9999	5,0036	5,0102	5,0205	5,0064	5,0201	4,9989	4,9991	4,9996
Reactor full	233,6	233,8	233,5	233,6	240,06	227,32	222,03	222,12	240,19	234,48	234,12	233,72
Reactor post reaction	233,67	233,8	233,49	233,6	240,08	227,37	222,11	222,18	240,19	234,5	234,11	233,77
Paper dry	1,2199	1,2221	1,5248	1,2399	1,404	2,0936	0,9979	0,6851	1,5268	0,989	0,9991	1,4472
Paper wet	1,2698	1,2681	1,5553	1,2696	1,4338	2,1125	1,0098	0,7489	1,5453	1,0389	1,0434	1,5366
Reactor without gas	233,47	233,61	233,34	233,48	239,91	227,22	222,01	222,04	240,09	234,31	233,91	233,54
Becher empty	32,4005	32,4538	32,4082	32,4015	32,3891	32,3828	32,3883	32,3883	32,4162	30,5607	32,3712	32,3904
Becher + water	35,4057	35,3248	35,6861	35,6757	35,7716	35,6381	36,0709	35,6775	35,7392	33,4877	35,0684	35,5981
Watch glass	26,25	12,6738	12,7264	26,2512	26,0226	17,0516	16,3051	12,6493	16,2382	32,7476	16,3452	12,7259
Water in watch glass	1,146	1,1459	1,2216	1,2218	1,0414	0,9188	1,4794	0,9911	1,4712	1,058	1,061	0,9883
Residue	26,2981	12,7183	12,7848	26,3081	26,0581	17,0871	16,3469	12,6937	16,2782	32,7893	16,3789	12,7613
Thimble + cotton	1,1821	1,3485	1,3966	1,1841	1,2054	1,2277	1,3422	1,2945	1,3656	1,4146	1,3591	1,404
Thimble + char	1,5623	1,7222	1,8066	1,5663	1,5884	1,6163	1,7149	1,6798	1,8011	1,7047	1,7258
Ball empty	71,4694	75,3458	73,255	71,4294	75,8391	75,8422	79,9539	71,4609	73,2532	71,4615	79,9849	79,9552
Ball + oil	71,6463	75,5133	73,4811	71,6452	76,0949	76,1065	80,2069	71,744	73,5213	71,7212	80,2058	80,2106
Reactor with char	227,8583	227,7438	227,7542	227,6581	234,0791	221,4212	216,4012	216,1625	227,7541	228,5026	216,4012	227,9218
Reactor cleaned	227,8353	227,7295	227,75	227,6353	234,0787	221,4188	216,3105	216,1608	227,7514	228,5001	216,3105	227,9122

II.II. At 300ºC

Table V. Summary of the experimental data obtained at 300°C.

	300ºC											
	A [3min+0min]	D [3min+0min]	C [3min+0min]	B [3min+10min]	B [3min+10min]	D [3min+10min]	B [3min+15min]	B [3min+15min]	A [3min+15min]	C [3min+20min]	A [3min+20min]	B [3min+20min]
	weight [g]	weight [g]	weight [g]	weight [g]	weight [g]	weight [g]	weight [g]	weight [g]	weight [g]	weight [g]	weight [g]	weight [g]
Reactor Empty	233,95	234,08	234,21	221,45	234,26	228,74	221,32	234,3	227,81	234,4	227,68	234,2
Biomass	1,0066	0,9988	0,9994	1,0075	1,0066	1,0032	0,9982	1,0062	0,9991	0,9998	1,0003	0,9992
Water	4,9931	4,9964	4,9992	5,0135	5,0692	5,0123	5,0105	5,0076	5,0099	5,0165	5,0739	5,0145
Reactor full	239,95	240,08	240,72	227,49	240,31	234,76	227,32	240,31	233,9	240,44	233,76	240,21
Reactor post reaction	239,95	240,08	240,71	227,47	240,35	234,76	227,35	240,39	233,9	240,43	233,67	240,21
Paper dry	1,2624	1,2706	1,7347	0,2896	2,1621	1,4378	1,1282	2,1884	1,1281	1,3292	2,1781	1,1282
Paper wet	1,3105	1,2896	1,8724	0,3	2,2149	1,5433	1,134	2,2437	1,1391	1,3489	2,1936	1,14
Reactor without gas	239,78	239,97	240,52	227,4	240,15	234,47	227,21	240,18	233,75	240,28	233,56	240,09
Becher empty	32,397	32,408	32,4742	32,3909	32,3951	32,4753	32,3893	32,3953	32,7437	32,3898	44,9183	32,7358
Becher + water	35,6129	35,7395	35,7723	36	35,7522	36,1242	35,7016	35,5496	36,0128	36,0017	48,487	36,3257
Watch glass	24,3745	25,7082	12,3476	12,6494	16,305	16,7238	26,0204	16,3052	12,7543	26,0551	26,2521	26,0591
Water in watch glass	1,0405	0,7888	0,7874	0,7163	0,9478	0,7165	0,9305	1,0562	0,9299	0,816	1,1665	0,8182
Residue	24,4136	25,7361	12,3698	12,6697	16,3549	16,7438	26,0503	16,3438	12,7741	26,0762	26,2863	26,0792
Thimble + cotton	1,2409	1,343	1,8745	1,259	1,3555	1,9358	1,279	1,3128	1,5837	1,2508	1,2549	1,1232
Thimble + char	1,7158	1,7446	2,2234	1,7423	1,6057	2,2813	1,6414	1,5759	1,9238	1,5507	1,614	1,4213
Ball empty	71,4676	79,9571	79,7283	75,8361	71,4837	79,4376	79,9551	79,9605	79,2672	71,4702	75,84	79,3252
Ball + oil	71,7224	80,2136	79,9734	76,0778	71,7587	79,6824	80,23	80,2755	79,5221	71,77	76,1105	79,6032
Reactor with char	0	233,8308	234,7442	200,9425	234,6933	234,9742	221,6119	234,5858	227,9124	0	228,2222	234,7623
Reactor cleaned	0	233,8124	234,7402	200,9133	234,693	234,9732	221,552	234,5426	227,9119	0	228,2018	234,7611

Table VI. Summary of the experimental data obtained at 300°C.

	300ºC					
	C [3min+25min]	C [3min+25min]	C [3min+25min]	D [3min+30min]	A [3min+30min]	A [3min+30min]
	weight [g]	weight [g]	weight [g]	weight [g]	weight [g]	weight [g]
Reactor Empty	227,78	219,16	227,54	227,55	227,79	227,77
Biomass	1,0011	1,0021	1,0018	0,9999	0,9965	1,003
Water	5,0109	5,0087	5,0121	5,0071	5,0082	5,0132
Reactor full	233,79	225,15	233,52	233,55	233,81	233,77
Reactor post reaction	233,79	225,18	233,55	233,55	233,81	233,52
Paper dry	1,2348	1,0004	0,7056	0,9548	1,4866	2,1707
Paper wet	1,2499	1,0188	0,724	1,0342	1,5644	2,2462
Reactor without gas	233,61	225,02	233,38	233,38	233,6	233,27
Becher empty	32,38452	44,9124	32,39	32,1948	30,5596	32,3849
Becher + water	35,7724	48,3211	35,7747	35,7729	34,1623	35,3564
Watch glass	26,1034	26,0228	12,7264	12,7001	12,6495	26,0236
Water in watch glass	1,3201	1,2381	1,3195	0,7301	0,7288	1,0182
Residue	26,1611	26,0572	12,7817	12,7182	12,6686	26,0636
Thimble + cotton	1,1213	1,4479	1,2819	1,2198	1,3345	1,3946
Thimble + char	1,4715	1,7566	1,6578	1,6524	1,8225	1,6459
Ball empty	79,9346	73,2554	75,8359	75,6457	75,8363	85,2412
Ball + oil	80,1939	73,6032	76,097	75,8492	76,0182	85,5825
Reactor with char	227,9352	219,5276	227,79	227,7812	227,7438	228,2367
Reactor cleaned	227,9342	219,5231	227,7885	227,781	227,7295	228,2359

II.III. At 320ºC

Table VII. Summary of the experimental data obtained at 320°C.

	320ºC										
	[3min+0min]	[3min+0min] R	A [3min+0min]	B [3min+0min] R	[3min+5min]	[3min+5min] R	C [3min+5min]	[3min+10min]	D [3min+10min]	[3min+15min]	D [3min+15min]
	weight [g]	weight [g]	weight [g]	weight [g]	weight [g]	weight [g]	weight [g]	weight [g]	weight [g]	weight [g]	weight [g]
Reactor Empty	234,32	237,74	220,26	234,32	219,73	234,6	227,69	234,21	234,26	234,69	215,95
Biomass	1,0037	1,0007	1,0005	1,0036	1,0041	1	1,0008	0,9971	1,0052	1,0073	1,0014
Water	5,0404	5,0481	4,9931	4,9901	5,0209	5,02	5,019	5,0554	5,0428	4,9976	4,9903
Reactor full	240,36	243,79	226,28	240,37	225,75	240,63	233,7	240,26	240,71	240,68	221,96
Reactor post reaction	240,38	243,91	226,28	240,37	225,91	240,63	233,7	240,3	240,7	240,75	221,97
Paper dry	0,13	0,3213	1,6279	1,2352	0,2739	0,695	0,6932	0,2781	1,0623	0,3146	0,6292
Paper wet	0,341	0,3854	1,6394	1,2423	0,3196	0,7154	0,7125	0,313	1,1008	0,3336	0,6678
Reactor without gas	240,16	243,66	226,15	240,16	225,74	240,5	233,59	240,14	240,55	240,57	221,76
Becher empty	49,7548	49,7548	44,9028	34,2548	49,7548	46,5209	32,3852	46,27	32,3958	46,27	32,3873
Becher + water	53,0692	53,1327	47,9827	37,0892	53,16	49,9797	35,8121	49,65	35,7692	49,78	35,8327
Watch glass	0	0	16,3023	16,3252	0	16,3061	16,3471	12,725	16,2196	18,4023	18,4082
Water in watch glass	0	0	1,5463	1,5501	0	0,7454	0,7419	1,2646	1,2611	1,0979	0,9907
Residue	0	0	16,3817	16,3756	0	16,3263	16,3672	12,7528	16,2478	18,4268	18,4118
Thimble + cotton	1,4406	1,4406	1,2582	1,5935	1,2756	1,9223	1,3927	1,2145	1,1279	1,3207	1,3772
Thimble + char	2,348	2,348	1,6532	2,0121	1,7088	2,3238	1,7962	1,6427	1,5571	1,7396	1,7796
Ball empty	75,8295	75,8295	79,2375	79,8385	79,9557	75,8392	79,9653	45,9332	79,6813	61,6927	79,9515
Ball + oil	76,1607	76,1607	79,3932	80,0225	80,1871	76,0461	80,1734	46,157	79,9026	61,9183	80,1564
Reactor with char	210,1238	210,6084	220,3521	210,6084	200,0594	186,3565	228,439	210,1145	234,7142	186,3067	209,972
Reactor cleaned	210,1062	210,5773	220,3511	210,5773	200,0432	186,3041	228,4312	210,1024	234,7118	186,2995	209,8981

Table VIII. Summary of the experimental data obtained at 320°C.

	320ºC										
	[3min+15min]	[3min+20min]	A [3min+20min]	B [3min+20min]	D [3min+25min]	[3min+30min]	C [3min+30min]	[3min+45min]	[3min+45min] R	D [3min+25min]	[3min+30min]
	weight [g]	weight [g]	weight [g]	weight [g]	weight [g]	weight [g]	weight [g]	weight [g]	weight [g]	weight [g]	weight [g]
Reactor Empty	234,69	234,41	227,71	227,71	234,7	218,44	228,47	234,31	234,64	234,24	234,7
Biomass	1,0003	1,0017	1,0005	1,0005	1,0001	0,99	1,02	0,997	1	1,0006	1,0001
Water	4,9991	5,0118	5,0121	5,0121	5,0101	4,99	5,0088	5,2385	5	5,0099	5,0101
Reactor full	240,69	240,42	233,72	233,72	240,69	224,42	234,5	240,55	240,64	240,29	240,69
Reactor post reaction	240,69	240,45	233,72	233,72	240,69	224,42	234,32	240,55	240,64	240,29	240,69
Paper dry	1,3172	0,5586	1,0625	1,0625	1,1448	0,2484	1,0399	0,4821	0,7965	1,1448	1,2342
Paper wet	1,3368	0,6305	1,1329	1,1329	1,2115	0,2881	1,0747	0,5309	0,8909	1,2115	1,2781
Reactor without gas	240,52	240,25	233,57	233,57	240,48	224,29	234,2	240,34	240,4	240,12	240,58
Becher empty	32,8724	47,6009	32,5374	32,5374	32,3893	46,2879	32,3879	33,26	46,2905	32,3578	32,4234
Becher + water	35,4692	50,9069	35,8371	35,8371	35,4703	49,5897	35,6283	36,7511	49,7225	35,4603	35,6383
Watch glass	16,3532	12,7263	16,4362	16,4362	26,0535	17,0512	26,2511	4,7445	12,6498	26,2348	17,0512
Water in watch glass	1,0983	1,345	1,3474	1,3474	1,2976	0,7785	1,1182	0,8765	0,684	1,2301	0,7695
Residue	16,3778	12,7595	16,4691	16,4691	26,0976	17,0641	26,285	4,7625	12,6594	26,2841	17,0641
Thimble + cotton	1,3646	1,5493	1,4573	1,4573	3,67	1,5348	1,3346	1,3656	1,4312	1,5436	1,3485
Thimble + char	1,7916	1,95	1,8533	1,8533	4,0595	1,9265	1,725	1,7862	1,8404	1,8847	1,7265
Ball empty	79,7563	79,955	79,9631	79,9631	75,8518	79,9513	79,9484	79,9619	75,8381	75,8857	79,9513
Ball + oil	79,9735	80,2118	80,2271	80,2271	76,0606	80,2036	80,184	80,1908	76,0624	76,1347	80,1876
Reactor with char	234,8123	210,055	228,3782	228,3782	234,7791	179,773	228,5378	210,1558	210,5742	234,7745	179,773
Reactor cleaned	234,8103	210,028	228,3723	228,3723	234,7782	179,7646	228,5369	210,1373	210,5573	234,7742	179,7646

APPENDIX 3: YIELDS TABLE

III.I. At 280ºC [% db]

Table IX. Evolution of yields and their standard deviations during the process at 280 °C as a function of time.

Time (min)	0	5	10	20	30
Biocrude 280 °C	17,2	22,0	26,0	26,9	24,4
Solid Residue 280 °C	39,5	40,8	38,7	40,7	38,3
Water Soluble Organics 280 °C	20,3	23,5	18,2	16,8	17,7
Gaseous Phase 280 °C	14,7	10,5	13,6	8,22	14,5
Dev BC 280 °C	0,463	0,511	0,374	1,17	1,76
Dev S 280 °C	0,744	0,454	0,304	4,26	4,14
Dev WSO 280 °C	0,794	0,298	1,11	3,98	1,54
Dev G 280 °C	0,299	1,45	0,481	0,507	0,698

III.II. At 300ºC [% db]

Table X. Evolution of yields and their standard deviations during the process at 300 °C as a function of time.

Time (min)	0	10	15	20	25	30
Biocrude yield 300 °C	25,2	25,2	28,1	28,3	28,9	19,3
Solid residue 300 °C	41,5	36,8	35,6	32,6	34,7	46,8
Water soluble organics 300 °C	16,8	18,2	15,0	13,4	18,9	12,8
Gaseous phase 300 °C	8,82	13,0	14,2	11,1	15,2	11,2
Dev bc 300 °C	0,482	1,48	2,40	1,25	4,11	1,05
Dev sr 300 °C	4,86	4,83	4,96	3,75	2,64	3,56
Dev wso 300 °C	1,95	5,89	3,17	1,08	3,57	0,378
Dev gp 300 °C	2,82	1,88	0,822	1,48	0,959	2,10

III.III. At 320ºC [% db]

Table XI. Evolution of yields and their standard deviations during the process at 320 °C as a function of time.

Time (min)	0	5	10	15	20	25	30
Biocrude yield 320 °C	16,74	21,51	22,23	21,52	26,14	22,88	24,07
Solid residue 320 °C	44,34	43,75	43,55	44,25	41,01	36,58	39,14
Water soluble organics 320 °C	20,90	13,60	11,18	8,03	12,27	18,55	10,55
Gaseous phase 320 °C	12,88	10,80	11,82	16,04	9,57	12,33	8,03
Dev bc 320 °C	1,00	1,09	0,21	0,80	0,35	2,00	1,02
Dev sr 320 °C	2,85	1,89	0,61	2,35	1,19	2,46	0,91
Dev wso 320 °C	4,73	0,01	0,04	4,39	0,06	1,52	3,07
Dev gp 320 °C	3,62	1,36	0,73	0,85	2,28	2,00	1,05

APPENDIX 4: COMPOSITION OF SEWAGE SLUDGE TABLE

Table XII. Summary of the experimental data obtained for the composition of sewage sludge from a wastewater treatment plant in Rome.

	weight [g]
Reactor Empty	227,35
Biomass	0,999
Water	4,9934
Reactor full	233,35
Reactor post reaction	233,37
Becher empty	32,3877
Becher + water	35,6554
Watch glass	26,0531
Water in watch glass	0,8764
Residue	26,0988
Thimble + cotton	3,4928
Thimble + biomass	4,455
Ball empty	71,4562
Ball + oil	71,6271

HTL 200ºC + 2nd Extraction (Methanol+Hexane) 20 min	
LIPIDS	1
Biomass before R	0,999
Water	4,9934
Biomass	0,9622
Ditale + res	4,455
Ditale + res 2	4,232
Lipids ballone	0,177613802
Lipids totale	0,2008
Lipids diference	0,2318

APPENDIX 5: MASS FLOW TABLE FROM SIMULATION

Table XIII. Summary of the mass flows of the reactants and products obtained at different reaction temperatures from the simulations in Aspen Plus v12.

T (ºC)	Mass Flow [kg/h]						
	(1) Biomass	(2) Water	(3) Feed	(4) Gaseous	(5) BC	(6) WSO	(7) Char
250	6240	31200	37440	0	887	550	550
275	6240	31200	37440	0	1891	1267	1267
300	6240	31200	37440	1	2898	2392	2392
325	6240	31200	37440	4	2516	3585	3585
350	6240	31200	37440	12	1888	4242	4242
400	6240	31200	37440	53	1646	2838	2838